

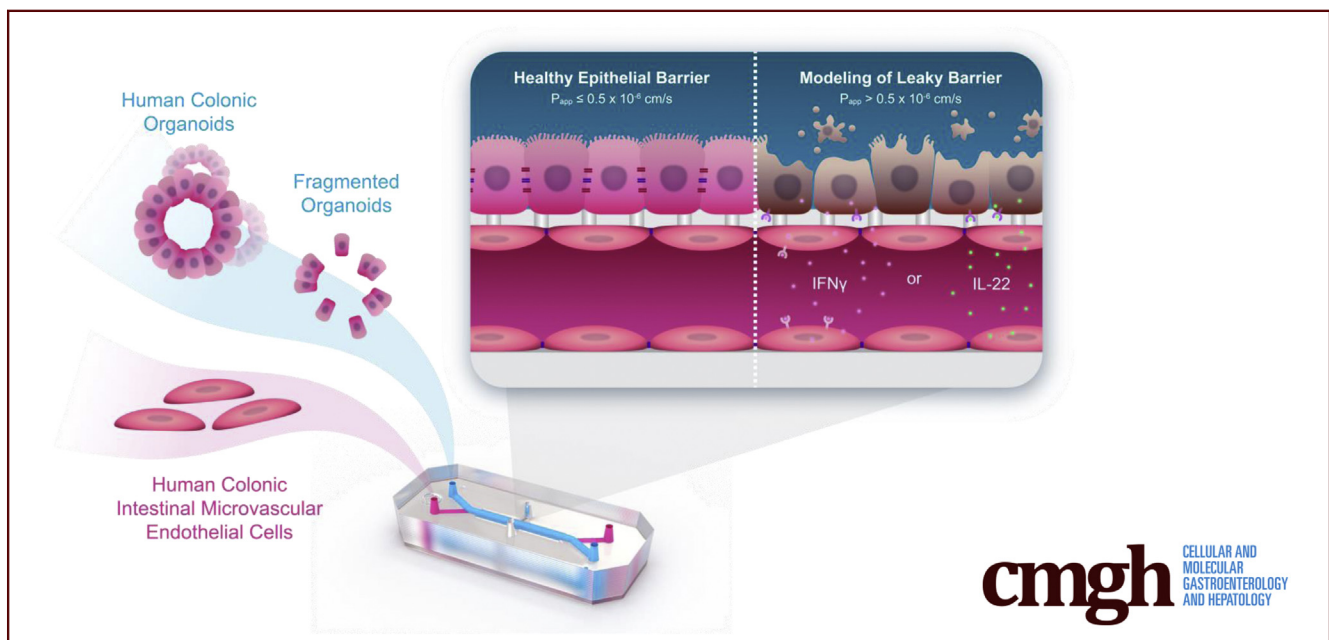
ORIGINAL RESEARCH

A Novel Microphysiological Colon Platform to Decipher Mechanisms Driving Human Intestinal Permeability



Athanasia Apostolou,^{1,2} Rohit A. Panchakshari,^{3,§} Antara Banerjee,^{3,§} Dimitris V. Manatakis,¹ Maria D. Paraskevopoulou,⁴ Raymond Luc,¹ Galeb Abu-Ali,⁴ Alexandra Dimitriou,¹ Carolina Lucchesi,¹ Gauri Kulkarni,¹ Tengku Ibrahim Maulana,^{1,5} Magdalena Kasendra,¹ Jordan S. Kerns,¹ Bertram Bleck,⁴ Lorna Ewart,¹ Elias S. Manolagos,^{6,7} Geraldine A. Hamilton,¹ Cosmas Giallourakis,⁴ and Katia Karalis¹

¹Emulate, Inc, Boston, Massachusetts; ²Department of Medicine, School of Health Sciences, National and Kapodistrian University of Athens, Athens, Greece; ³Takeda California, Inc, San Diego, California; ⁴Takeda Pharmaceuticals, Ltd, Cambridge, Massachusetts; ⁵Faculty of Energy, Process and Bioengineering, Department of Bioengineering, University of Stuttgart, Stuttgart, Germany; ⁶Department of Informatics and Telecommunications, National and Kapodistrian University of Athens, Athens, Greece; and ⁷Northeastern University, Boston, Massachusetts



SUMMARY

Colon Intestine-Chip (Emulate, Inc, Boston, MA), seeded with human colon crypt-derived epithelial and primary microvascular endothelial cells, was built to investigate leaky gut in human beings. This *ex vivo* platform recapitulated the effects of proinflammatory cytokines in the intestinal epithelial barrier and identified novel mechanisms of action.

BACKGROUND & AIMS: The limited availability of organoid systems that mimic the molecular signatures and architecture of human intestinal epithelium has been an impediment to allowing them to be harnessed for the development of therapeutics as well as physiological insights. We developed a microphysiological Organ-on-Chip (Emulate, Inc, Boston, MA)

platform designed to mimic properties of human intestinal epithelium leading to insights into barrier integrity.

METHODS: We combined the human biopsy-derived leucine-rich repeat-containing G-protein-coupled receptor 5-positive organoids and Organ-on-Chip technologies to establish a micro-engineered human Colon Intestine-Chip (Emulate, Inc, Boston, MA). We characterized the proximity of the model to human tissue and organoids maintained in suspension by RNA sequencing analysis, and their differentiation to intestinal epithelial cells on the Colon Intestine-Chip under variable conditions. Furthermore, organoids from different donors were evaluated to understand variability in the system. Our system was applied to understanding the epithelial barrier and characterizing mechanisms driving the cytokine-induced barrier disruption.

RESULTS: Our data highlight the importance of the endothelium and the *in vivo* tissue-relevant dynamic microenvironment

in the Colon Intestine-Chip in the establishment of a tight monolayer of differentiated, polarized, organoid-derived intestinal epithelial cells. We confirmed the effect of interferon- γ on the colonic barrier and identified reorganization of apical junctional complexes, and induction of apoptosis in the intestinal epithelial cells as mediating mechanisms. We show that in the human Colon Intestine-Chip exposure to interleukin 22 induces disruption of the barrier, unlike its described protective role in experimental colitis in mice.

CONCLUSIONS: We developed a human Colon Intestine-Chip platform and showed its value in the characterization of the mechanism of action of interleukin 22 in the human epithelial barrier. This system can be used to elucidate, in a time- and challenge-dependent manner, the mechanism driving the development of leaky gut in human beings and to identify associated biomarkers. (*Cell Mol Gastroenterol Hepatol* 2021; 12:1719–1741; <https://doi.org/10.1016/j.jcmgh.2021.07.004>)

Keywords: Organoids; Organ-on-Chip; Leaky Gut; Interleukin 22.

The gastrointestinal barrier is the most extensive epithelial barrier of the body that is colonized by commensal bacteria, segregated from the host's immune system to maintain homeostasis.¹ The characteristics of the intestinal barrier are attributed mainly to the epithelial cell interconnections via specialized tight junctions (TJs). Supporting elements include locally secreted factors, the mucin layer, and microbiome-derived humoral factors. Disruption of the barrier was first identified in infections and inflammatory bowel disease (IBD)²; with the list continuously expanding to include additional diseases, drugs, and toxic factors.^{3,4} Intestinal crypt stem cells renew the intestinal epithelial cells (IECs) during the lifespan, thus maintaining barrier function and enabling the repair of the injured barrier. Dysregulation of epithelial regeneration is critical for the progression of chronic gastrointestinal diseases.

The significance of cytokines in disruption, repair, or accelerated damage of the intestinal barrier has been shown both *in vivo* and in cell-based disease models. Mechanisms used by proinflammatory cytokines to disrupt the barrier include induction of epithelial cell apoptosis and degeneration of the TJs. Interferon- γ (IFN γ) is the prototype cytokine used, either alone or in combination with tumor necrosis factor α (TNF α) or interleukin (IL)1 β , to induce barrier disruption in several intestinal disease models. Specifically, prolonged exposure of IECs to IFN γ results in activation of apoptotic mechanisms,⁵ increased expression of Dickkopf-related protein 1 (DKK1) and inhibition of epithelial proliferation,⁶ or phosphorylation of Myosin-Light Chain (MLC) via activation of the Myosin-Light Chain Kinase (MLCK), which drives internalization and, thus, disruption of TJs.^{5,7}

A major advancement in our ability to understand the regulation of intestinal epithelial homeostasis has been the discovery of organoid technology.^{8,9} This development enables the use of patient-derived samples to capture the spectrum of individual responses¹⁰ and significantly advances our understanding of IEC biology. Recently, a culture


system was developed in Transwells that enables expansion of organoids to multicellular polarized monolayer epithelia and was applied to model intestinal infection.¹¹ This system bypasses the main caveat of the organoids, which is the lack of accessibility to the apical side of IECs, the equivalent of the luminal tissue side. A missing element of the earlier-described systems that is addressed by the Organ-on-Chip technology is the potential to incorporate conditions that emulate the intestinal microenvironment.^{12,13} Specifically for the gut, significant features include stretching to emulate the peristalsis-like motion of the tissue, exposure to shear stress, and interactions of the epithelium and endothelium or other cells via tissue-relevant extracellular matrix proteins. The Duodenum Intestine-Chip (Emulate, Inc, Boston, MA) supports the synchronous culture of different, tissue-relevant cell types of the intestinal lumen and, thus, enables functionality, such as the activity of CYP3A4, much closer to that measured *in vivo* compared with other systems.¹⁴

Similarly, in this work, we leveraged the Organ-on-Chip technology^{14–16} and the proprietary Human Emulation System (Emulate, Inc, Boston, MA) to develop a human Colon Intestine-Chip (Emulate, Inc, Boston, MA) platform including organoid-derived IECs and primary microvascular intestinal endothelial cells. First, we confirmed *in vivo* relevant cytoarchitecture and tissue-relative abundance of the key colon epithelial cell subtypes. Next, we showed the reproducibility of the system among 3 donors including the establishment of a tight epithelial barrier. The latter provided the basis for modeling the well-established IFN γ -elicited barrier disruption and assessed the effects of IL22 on epithelial integrity. We show that IL22, upon engaging its receptors expressed in the Colon Intestine-Chip, acts as a barrier-insulting cytokine, in line with recent publications.^{17–19} These findings considered together indicate that the Colon Intestine-Chip renders a promising human platform for studying intestinal epithelial barrier development and homeostasis. Considering the use of epithelial modulatory effectors such as IL22 in clinical trials for indications such as IBD (<https://clinicaltrials.gov/ct2/show/NCT03558152>),²⁰ it also will be of interest to further understand the relationship of model systems, such as ours, to clinical read outs.

In summary, we present the development of a new biopsy-derived Colon Intestine-Chip as a human organoid-

[§]Authors share co-senior authorship.

Abbreviations used in this paper: cHIMEC, colonic human intestinal microvascular endothelial cell; DGE, differential gene expression; DKK1, Dickkopf-related protein 1; ECM, extracellular matrix; EdU, 5-ethynyl-2'-deoxyuridine; GO, gene ontology; IBD, inflammatory bowel disease; IEC, intestinal epithelial cell; IFN γ , interferon- γ ; IL, interleukin 6; IL22BP, interleukin 22 binding protein; NHS, N-hydroxysuccinimide; P_{app}, apparent permeability; PBS, phosphate-buffered saline; PDMS, polydimethylsiloxane; qPCR, quantitative polymerase chain reaction; RNA-seq, RNA sequencing; STAT, signal transducer and activator of transcription; TJ, tight junction; TNF α , tumor necrosis factor α ; Wnt, wingless-related integration site; ZO-1, zonula occludens-1.

 Most current article

© 2021 The Authors. Published by Elsevier Inc. on behalf of the AGA Institute. This is an open access article under the CC BY-NC-ND license (<http://creativecommons.org/licenses/by-nc-nd/4.0/>).

2352-345X

<https://doi.org/10.1016/j.jcmgh.2021.07.004>

based platform to study cell–cell interactions. The Colon Intestine-Chip is a significant development for targeting unmet needs such as leaky barrier implicated in the pathogenesis of gastrointestinal diseases, toxicity by frequently used drugs, and aging.

Results

Development of a Colon Intestine-Chip Platform

As previously described, juxtaposed culture of intestinal epithelial and endothelial cells in micro-engineered Organ-Chips results in the formation of a 3-dimensional mucosal layer.¹³ Here, we applied this technology to develop a Colon Intestine-Chip based on human organoids isolated from colonic biopsy specimens, along with colon-specific microvascular endothelial cells (Figure 1A). The top and bottom surface of the membrane, precoated uniformly with extracellular matrix (ECM) proteins, as depicted by fluorescent staining with N-hydroxysuccinimide (NHS)-ester dye (Figure 1B), was seeded with enzymatically fragmented organoids and endothelial cells, respectively (Figure 1C). Culture conditions included fluid flow, supported by the Zoë Culture Module (Emulate, Inc) (see the Materials and Methods section for more detail), at 60 $\mu\text{L}/\text{h}$ initiated on day 1, followed by the removal of the stemness supporting factors, Y-27632 and CHIR99021, on day 2 of the culture (Figure 1D). Periodic stretch initiated on day 3 at 2% intensity and after 24 hours of pre-acclimation was switched to 10% until the completion of the study. The key point for switching to 10% stretching is when a confluent epithelial monolayer is established (Figures 2A and 3A), and the apparent permeability to 3 kilodaltons dextran becomes stabilized at less than $0.5 \times 10^{-6} \text{ cm}/\text{s}^{21}$ (Figures 2B and 3B). Twenty-four hours after exposure to 10% stretching (day 5), we characterized the formation of TJs in the expanded colonic epithelial monolayer by immunostaining for zonula occludens-1 (ZO-1) and E-cadherin (Figures 2C and 3C). Next, we evaluated the cell polarization by immunostaining on the same day of culture for ion channels such as the apically expressed SLC26A3,²² and the basolaterally expressed Na^+/K^+ adenosine triphosphatase transporter²³ (Figures 2D and 3D). These results show the establishment of a tight, polarized, human colonic epithelial monolayer by day 5 of the culture of colonic organoids in the Intestine-Chip. We show here the apparent epithelial permeability of chips maintained in culture for 8 days (Figure 2B), with reproducible and robust data across different donors. To date, we have maintained the culture for 12 days.

Role of the Endothelium in the Establishment of the Epithelial Barrier

In the Colon Intestine-Chip, we observed that co-culture with endothelial cells significantly enhanced the epithelial barrier integrity in a nonadditive manner, as indicated by the apparent permeability to 3 kilodaltons dextran (day 4, endothelium alone: $7.38 \times 10^{-6} \text{ cm}/\text{s}$ vs minus endothelium: $3.01 \times 10^{-6} \text{ cm}/\text{s}$ vs plus endothelium: $0.89 \times 10^{-6} \text{ cm}/\text{s}$) (Figures 2B and 3B). In line with this observation, a mature TJ network was established as early as day 5 and maintained up to day 8 of culture (Figures 2C, 3C, and 4A). On the

contrary, in the absence of endothelium, the TJs were poorly defined, and ZO-1 and E-cadherin staining showed proteins localized in the cytoplasm, rather than on the cell membrane, as expected in tight epithelial barriers (Figures 2C and 4A). These data suggest that the endothelium supports the establishment and the maturation/differentiation of IECs and highlights the advantages of dynamic co-culture systems. Furthermore, immunostaining against the basolateral and apical transporters, Na^+/K^+ adenosine triphosphatase and SLC26A3, respectively, showed the compromised epithelial cell polarity in the absence of endothelium (Figures 2D and 4B). On the other hand, stretching did not have a clear impact on the polarization of IECs (Figure 3D). The enhanced expression of the TJ-associated proteins, *Cdh1* and *Tjp1*, and the ion transporters, *Atp1a1* and *Slc26a3*, also was confirmed at the transcriptome level throughout the culture (Figure 4C and D). Parallel scanning electron microscopy analysis showed the formation of a mature brush border, with densely packed microvilli, only in IECs co-cultured with endothelium (Figures 2E and F, 3E and F, and 4E and F).

To comprehensively characterize the co-culture effects on the colonoids and endothelial cells at a transcriptome level, we performed RNA sequencing (RNA-seq) analysis of colonoids cultured in suspension and colonoid-derived IECs on-Chip, in the presence and absence of endothelium and/or stretch. Principal component analysis used on the highly variable genes across libraries showed distinct gene expression profiles between the different on-Chip culture conditions and colonoids in suspension. Our data highlight the effect of endothelium on the divergence of the transcriptome of colonic IECs cultured on-Chip as opposed to colonoids in suspension (Figure 5A and B). We performed functional analysis on the 573 Differentially Expressed Genes and 881 Differentially Expressed Genes, identified of the 58,342 genes annotated in the genome between IECs cultured with or without endothelium in the presence of stretch, on days 5 and 8 of culture, respectively (Figure 5C and D). Significantly enriched terms related to cell development and morphogenesis, cytoskeletal remodeling, and mechanosensory behavior were identified over the course of the culture (Figure 5E and F). Linear differential gene expression analysis confirmed the role of the endothelium as a differentiation driving factor at various time points of experimentation (Figure 5G–I). These findings are consistent with the aforementioned experimental readouts because the increased expression of *Alpi* transcripts in colonocytes cultured juxtaposed to the endothelium (Figure 6D), complementing the scanning electron microscopy analysis (Figure 2E and F). At the transcriptome level, the application of stretch enhanced terms related to ion, lipoprotein, and water transportation, highlighting the importance of tissue-relevant mechanical forces for the functional maturation of the organoid-derived epithelial cells (Figure 5J–M).

Multilineage Differentiation of Colonoids in the Colon Intestine-Chip

Because the use of organoids in research is rapidly expanding, several protocols have been developed for

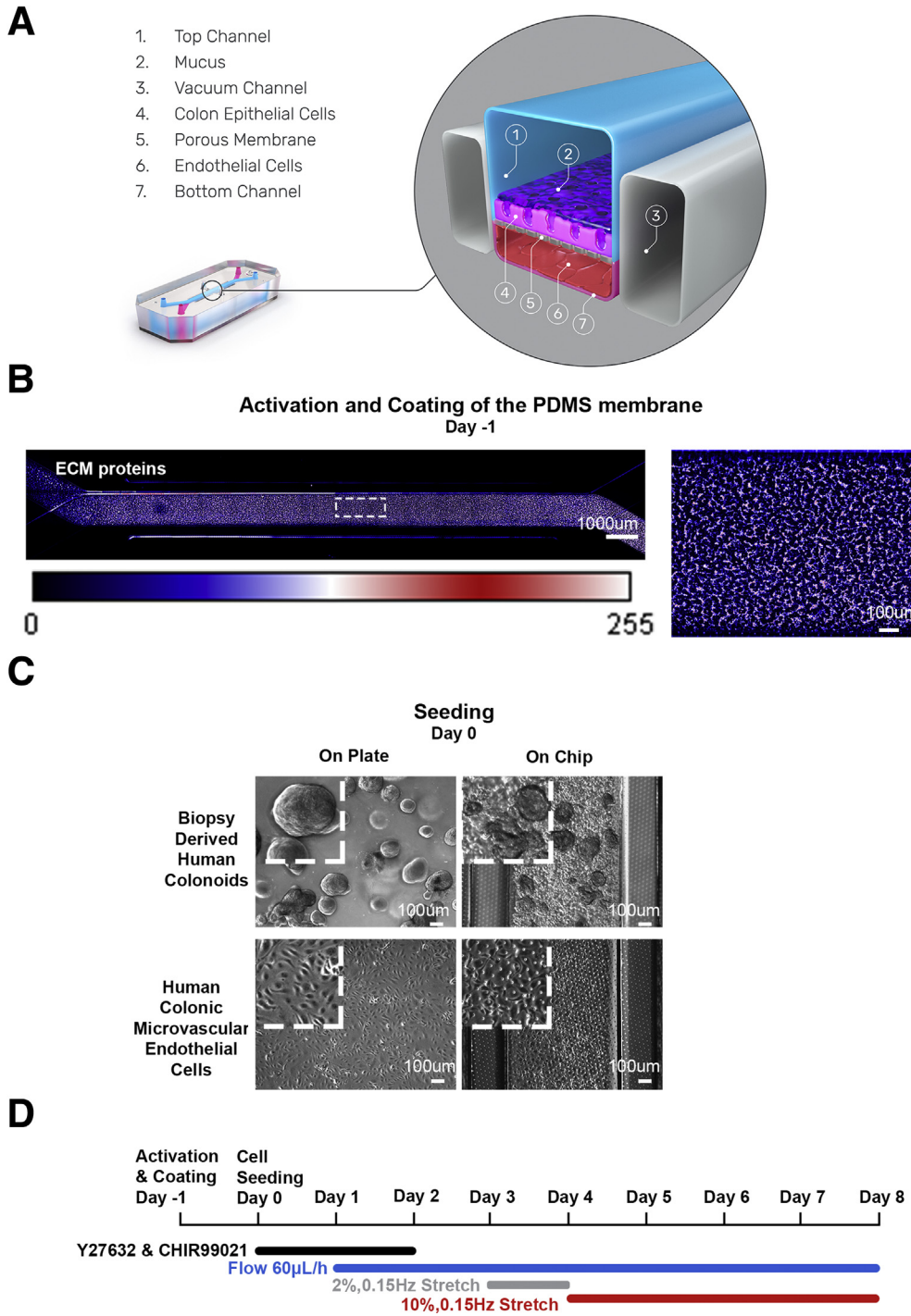
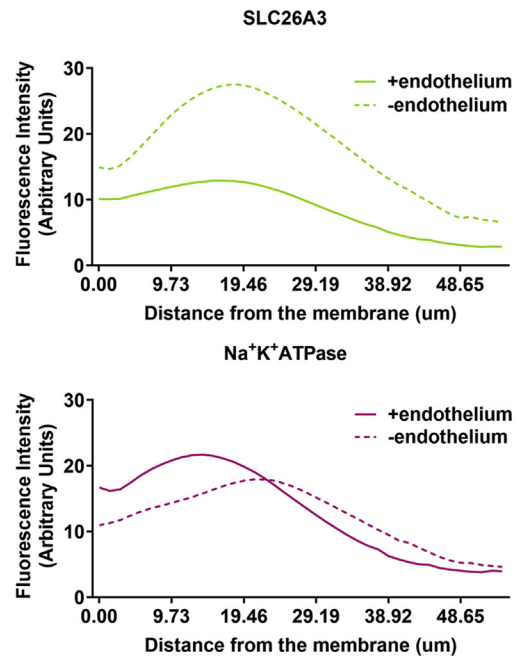
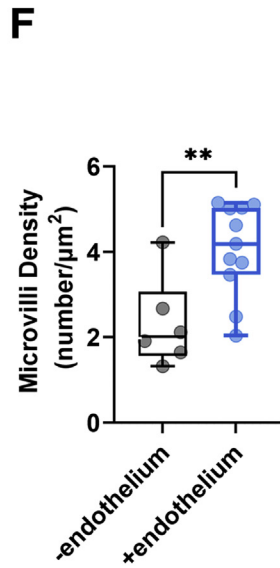
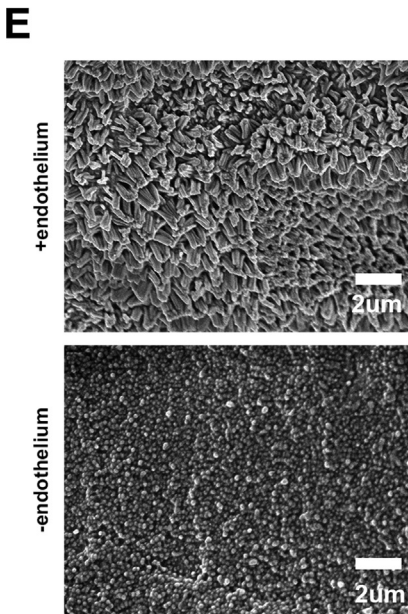
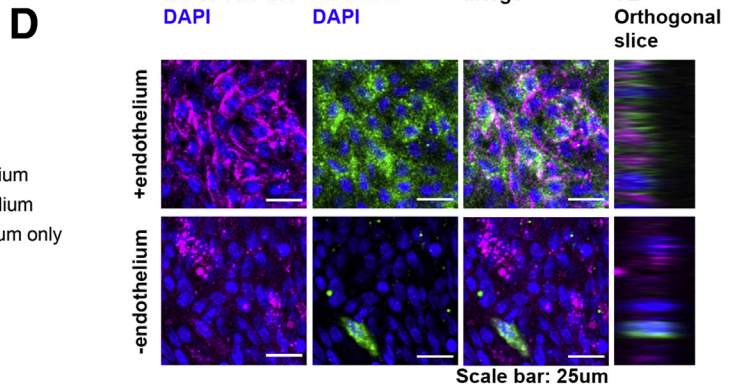
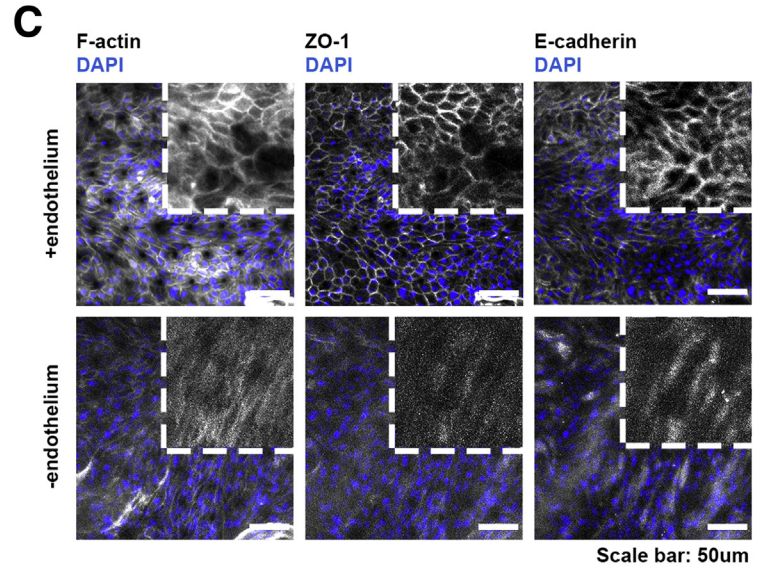
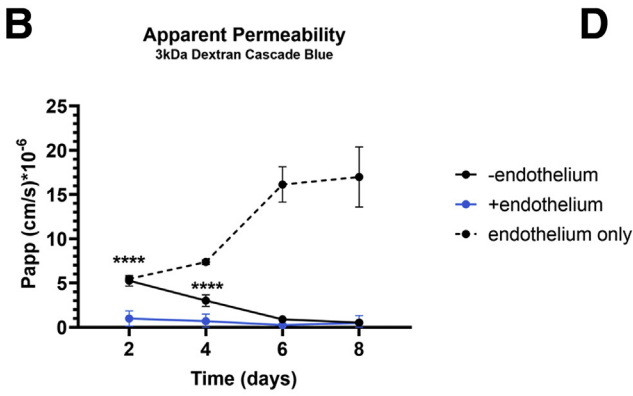
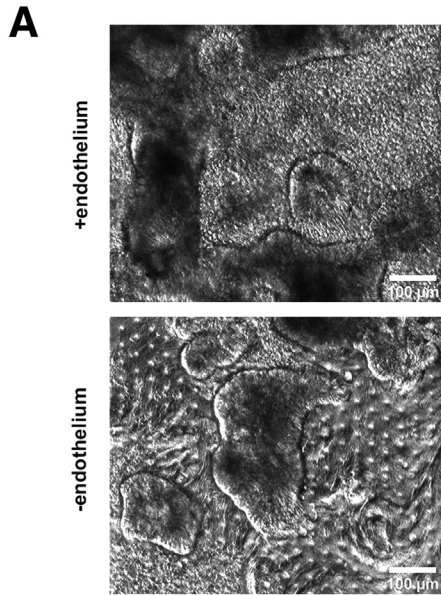


Figure 1. Establishment of the Colon Intestine-Chip. (A) Cross-section of the Colon Intestine-Chip showing the epithelial channel (1), mucus layer (2), vacuum chambers (3), colonic IECs (4), PDMS membrane (5), cHIMECs (6), and endothelial channel (7). (B) NHS-ester dye staining against the ECM proteins of the apical channel and the respecting Look Up Table color bar, representing the values of an 8-bit image pixel intensity. (C) Representative contrast-phase microscopy images of each cell type morphology, on a plate culture (left) and in the Colon Intestine-Chip (right), on day 0 of the culture. (D) Experimental timeline of the 8-day fluidic culture.

differentiation of the intestinal organoid-derived cells toward mature cells of absorptive and secretory lineage. These methods are based either on engraftment of the organoids in animals,²⁴ or in supporting signaling pathways required to define cell fate in the crypt-villus axis. In the latter, activation of wingless-related integration site (Wnt) and inhibition of p38 pathways²⁵ are the main options, often coupled with inhibition of the Notch pathway.²⁶ In the current study, the stemness factors, Wnt-3a/epithelial growth factor/noggin/R-spondin 1, were maintained in

the culture medium over the length of the culture. Immunofluorescence analysis on day 8 of culture shows physiological differentiation of the colonoid-derived IECs, toward absorptive enterocytes, goblet cells, and enteroendocrine cells (Figure 6A). This finding was verified by quantitative polymerase chain reaction (qPCR) and RNA-seq analysis for markers specific for the absorptive (*Alpi*) and secretory (*Muc2*, *ChgA*) subsets (Figure 6B and C). The presence of endothelium promoted the acquisition of a mature epithelial phenotype (Figure 6D). As can be deduced, the multilineage



differentiation occurred at the expense of the proliferating cells. Reduced expression of the cycling intestinal stem cell marker, *Lgr5*, over the course of the culture (Figure 6B), and drastic elimination of 5-ethynyl-2'-deoxyuridine (EdU)-positive cells by day 5 of culture (Figure 6E), are in further support of the gradual depletion of progenitor cells in the organoid-derived monolayer of IECs. Importantly, the Colon Intestine-Chips recapitulated the expected donor-to-donor variability in the differentiation process, as shown by the varying representation of the absorptive and secretory lineage among 3 different healthy individuals. Notably, donors presented with higher proliferative capacity had lower differentiation toward the absorptive phenotype, and vice versa (Figure 6A and E).

Barrier Disruption Model in the Colon Intestine-Chip

The intestinal barrier maintains mucosal homeostasis via compartmentalization of the resident commensal bacteria from the host immune cells. Disruption of the epithelial barrier results in activation of immune cells and cytokine release, propagating the epithelial injury. IFN γ , a type II IFN produced in the intestinal lamina propria, has been implicated in the pathogenesis of IBD.²⁷ Early studies showed the ability of IFN γ to compromise the intestinal epithelial barrier.⁷ Here, to simulate the *in vivo* action of IFN γ , we exposed the basolateral side of the epithelium to different concentrations of fluidically administered IFN γ in the endothelial channel (bottom channel) of the Colon Intestine-Chip. Two days after stimulation, we observed morphologic changes in the IECs (Figure 7A, red arrows), together with an associated concentration-dependent increase in the apparent permeability (P_{app}) to 3 kilodaltons of dextran (Figure 7B). The basolateral challenge of the IECs with IFN γ increased caspase 3 cleavage and activity (Figure 7C), while prolonged exposure to IFN γ resulted in decreased abundance of IECs (Figure 7D). Fluorescent staining for F-actin showed compromised cytoarchitecture, depicted by poorly defined cell borders and the appearance of enlarged, squamous-shaped cells (Figure 7E) and displaced localization of the TJ proteins ZO-1 and claudin 4 (red arrows).

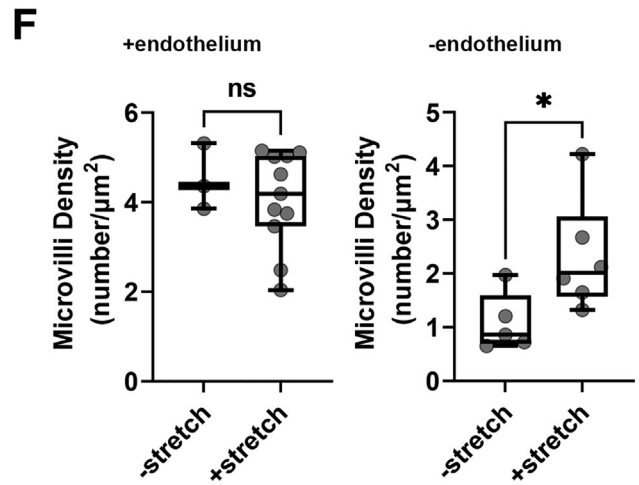
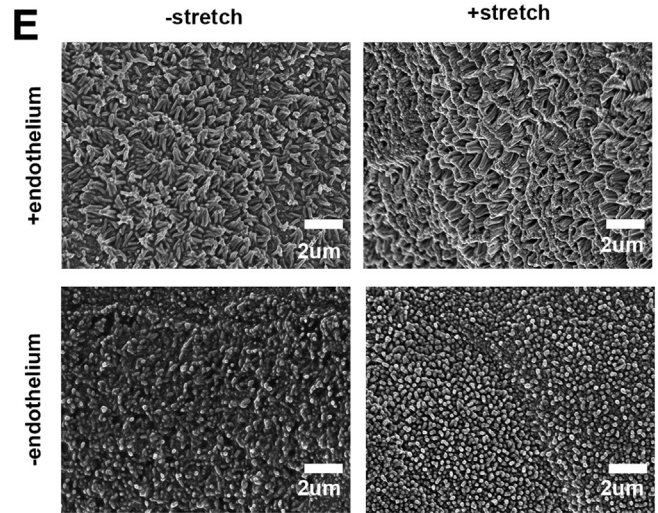
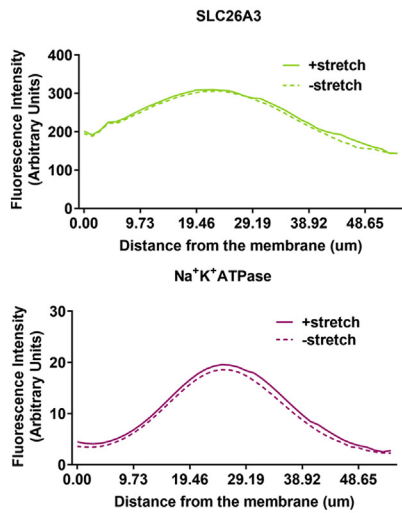
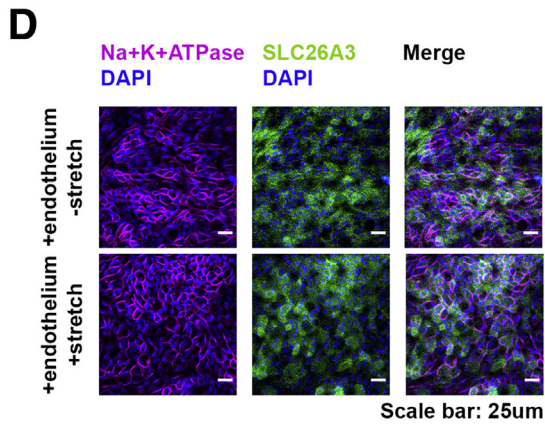
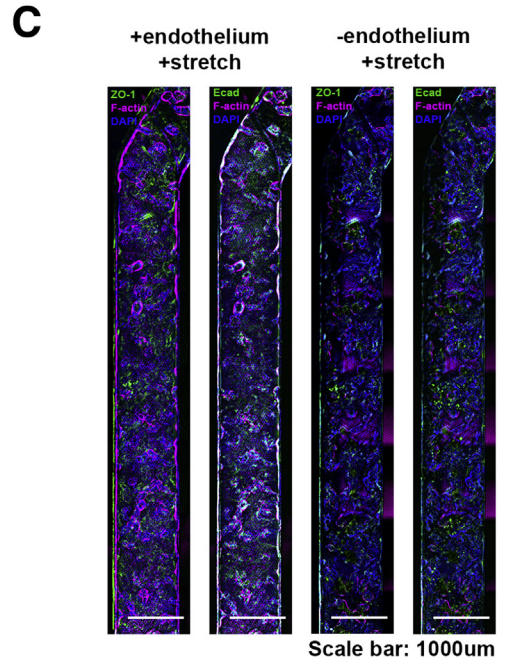
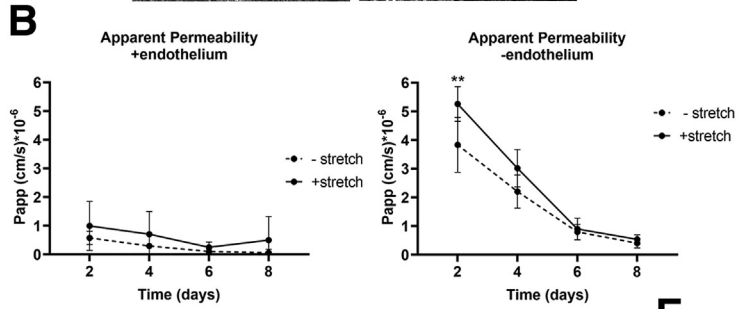
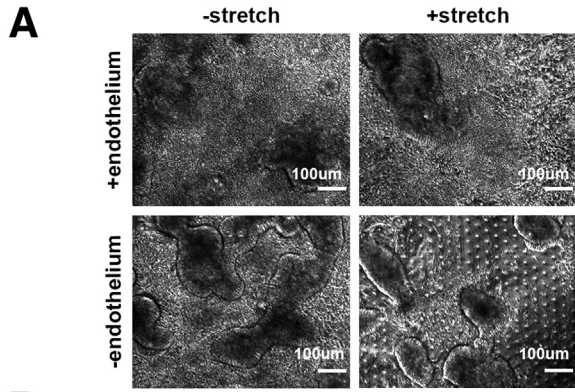
Expression of E-cadherin and occludin was reduced in TJs, in contrast to an increase in the cytoplasmic expression (red arrows). This finding is reminiscent of findings after cotreatment of T84 cells with IFN γ and tumor necrosis factor α , in which reduced affiliation of occludin, junctional adhesion molecule 1, and E-cadherin with membrane lipid rafts triggered redistribution of TJs and weakened cell-cell adhesion.²⁸ Furthermore, upon 24 hours of stimulation with IFN γ , we detected increased levels of IL6 and vascular cell adhesion molecule-1 in the effluent of the vascular channel (Figure 7F). Interestingly, intercellular cell adhesion molecule-1²⁹ and serum amyloid A³⁰ were detectable in the effluent of the top channel (Figure 7G), as reported for the sera of patients with inflammation.²⁹

IL22 Acts as a Barrier-Disruptive Agent for the Mature Colonic Epithelial Monolayer in the Colon Intestine-Chip

Because IL22, a cytokine implicated in IBD, has been shown to protect but also to worsen colitis in different mouse models,^{31,32} we sought to assess its effects in the Colon Chip, a human platform. The binding of IL22 to its receptor at the basolateral side of IECs³³ triggers the phosphorylation of signal transducer and activator of transcription (STAT)3.³⁴ We first confirmed the expression of the 2 IL22-receptor subunits, *Il22ra1* and *Il10rb*, in RNA-seq from organoid-derived IECs (Figure 8A). Interestingly, the expression of both *Il22ra1* and *Il10rb* was higher in the organoid-derived IECs in the chip compared with organoids in suspension culture, and was enhanced further in the presence of endothelium. These data signify the supportive effects of endothelium and the potentially incomplete understanding of human IL22 biology in the absence of a tissue-relevant microenvironment as in suspension cultures.¹⁹

Next, we stimulated the IECs in the Colon Intestine-Chip through the vascular channel with either 0.1, 0.3, or 1 nmol/L of IL22 in the presence or absence of IL22BP, for 1 hour, to determine the optimal concentration, resulting in activation of STAT3 (Figure 8B). The activation of STAT3 was maximal in the acute phase of treatment (1 h),

Figure 2. (See previous page). The presence of endothelium enhances the establishment of the epithelial barrier. (A) Representative phase-contrast images of the colonic epithelial cells on day 5 of the Colon Intestine-Chip culture in the presence or absence of endothelial cells. **(B)** The P_{app} to 3 kilodaltons dextran Cascade blue, of endothelial or epithelial cells, where stretch (10% strain, 0.15 Hz) was applied in the presence or absence of endothelium, over the course of an 8-day culture. Data shown correspond to 1 representative of 3 independent experiments. $n = 3-11$ chips/condition, means \pm 95% CI, 2-way analysis of variance, Tukey post hoc test. **(C)** Representative confocal fluorescent images showing the establishment of strong epithelial TJs on day 5 of culture in the presence of endothelium. TJs were stained with anti-ZO-1 and anti-E-cadherin and cytoskeleton with phalloidin (gray). Cell nuclei are shown in blue. **(D)** Representative confocal immunofluorescence images against the basolateral transporter Na⁺K⁺ adenosine triphosphatase (ATPase) (magenta) and the apical transporter SLC26A3 (green), indicating the establishment of a polarized epithelial monolayer on day 5 of culture only during the co-culture of colonocytes with endothelium. Cell nuclei are shown in blue. The plots indicate the mean fluorescent intensity distribution for each channel along the basal-apical axis of the epithelial cells. The quantification was performed across 3 different fields of view in 3 individual chips for each condition. **(E)** Representative scanning electron microscopy (SEM) images of the colonic epithelial cells on day 5 of the Colon Intestine-Chip culture, indicating maturation of the epithelial brush border in the presence of endothelial cells. **(F)** Box plots showing the density of microvilli per μm^2 , according to quantification of SEM images on day 5 of culture. The presence of endothelium significantly increases the density of microvilli per μm^2 . The quantification was performed across 6-11 different fields of view for each condition. Each individual point represents a single field of view. Unpaired *t* test. ***P* < .01 and *****P* < .0001. DAPI, 4',6-diamidino-2-phenylindole.



whereas it still was evident up to 72 hours after stimulation (Figure 8C), indicating the sustained sensitivity and responsiveness of the system for potential secondary readouts. Unlike the downstream effects of IL22, treatment with IFN γ did not result in significant activation of STAT3, highlighting the specificity of the event (Figure 8D).

IL12 and IL23 regulate IL22 and are central to the pathogenesis of IBD. The exact role and directionality of the IL22 effects in intestinal epithelial homeostasis are not clearly defined. Current reports include anti-inflammatory effects, induction of homeostatic factors or IEC proliferation,³⁵ as well as a reduction in epithelial integrity in mouse models or the Caco2 cells.^{17,18} Interestingly, a recent study showed induction of endoplasmic reticulum stress response in healthy and IBD colonoid-derived IECs.¹⁹ We next assessed the effects of IL22 on the epithelial permeability of the Colon Intestine-Chip, as described earlier, with the reproducible effects of IFN γ . As shown, challenge with 1 nmol/L IL22 for 48 hours resulted in compromised morphology of the epithelial monolayer (Figure 8E), with poorly defined cell borders and an increased number of floating cells in the effluent medium. We also detected increased P_{app} of the colonic epithelium to 3 kilodaltons of dextran, abrogated when co-treated with 30 nmol/L IL22BP (Figure 8F). Moreover, cleavage of caspase 3 was increased by IL22 (Figure 8G), likely affecting apoptosis in a similar way to IFN γ (Figure 8H). Transcriptomic analysis and downstream functional characterization of the differentially regulated genes support these data (Figure 8I and J). Functional enrichment of gene ontology (GO) terms indicated significant enrichment of biological processes associated with apoptosis and inflammatory responses (Figure 8K). Importantly, our data strongly suggest that IL22 targets human colonic epithelial cells to disrupt the barrier function, acting as an injurious factor.^{36,37} Notably, the IL22-driven effects shown with the Colon Intestine-Chip refer to an epithelium–endothelium system at a healthy state, in which healthy subjects have been stratified as a cell source

and cells have not been exposed previously to other inflammatory insults.

Discussion

Gastrointestinal diseases affect all ages and account for a significant part of acute and chronic diseases across the world. More than 11% of the US population is estimated to suffer from a digestive disorder, often compromising the quality of life or is associated with decreased life expectancy.³⁸ Despite advancements in population screening and improved diagnostic methods,³⁸ the treatment for a number of these diseases remain an unmet need.

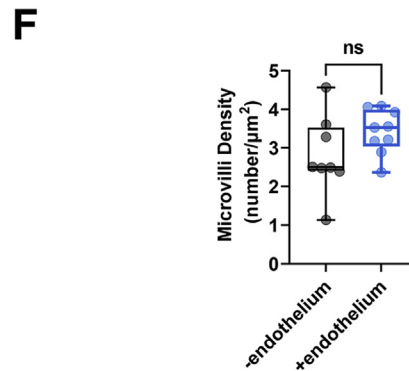
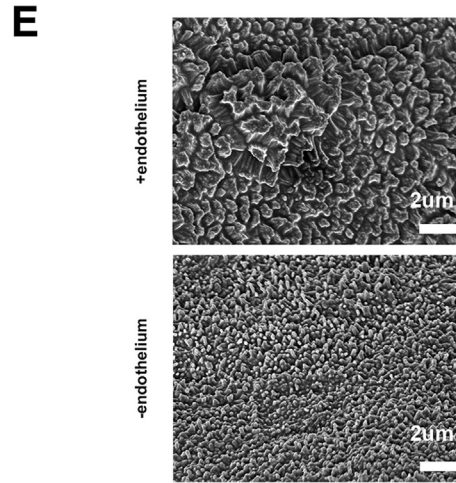
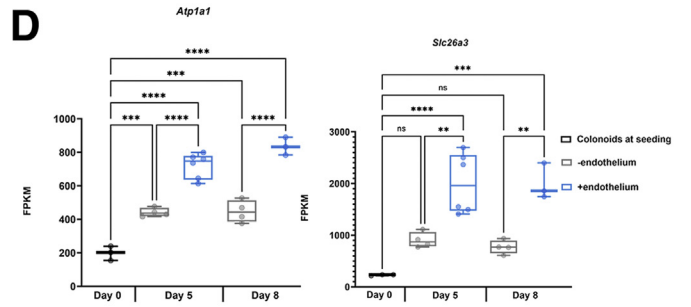
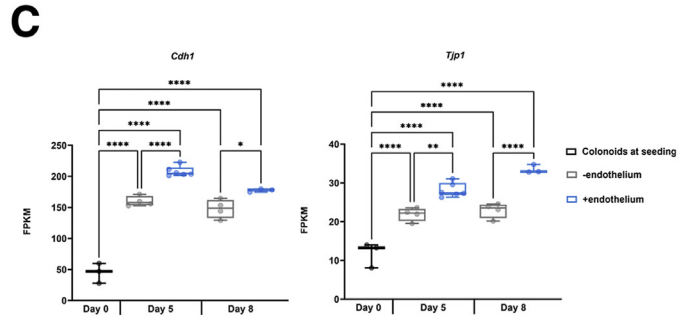
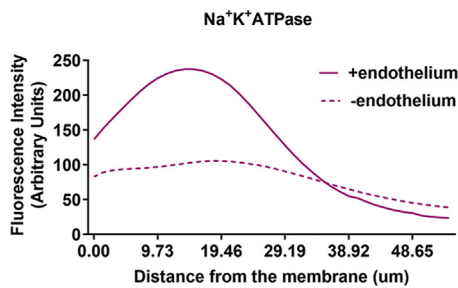
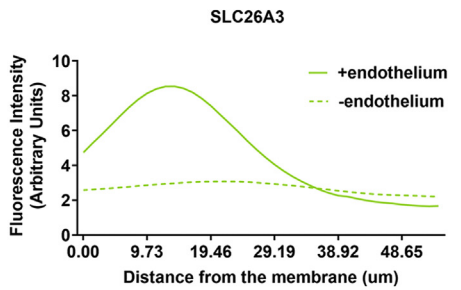
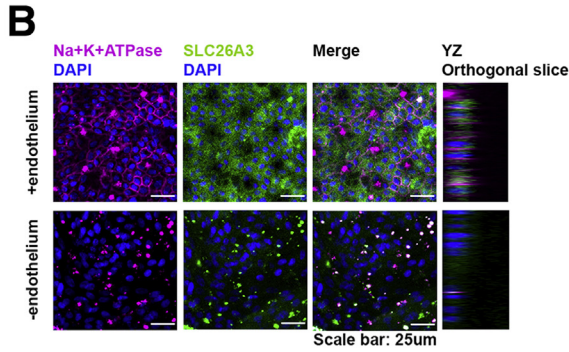
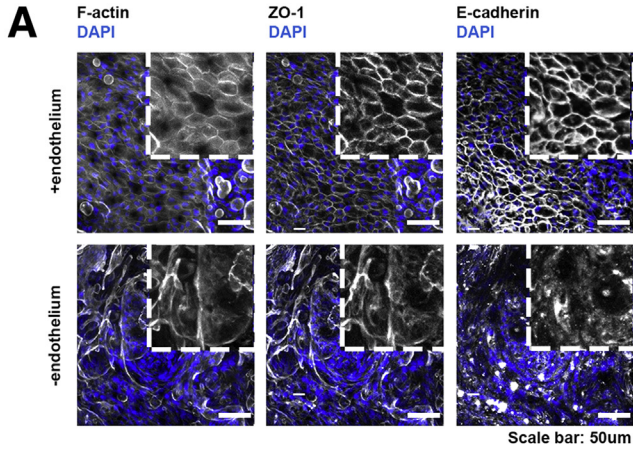
Intestinal epithelial homeostasis is intimately linked to the development of a tight epithelial barrier, owing to the specialized TJs connecting adjacent polarized IECs and associated supporting factors, such as the mucin layer. The significance of the barrier function is shown by the devastating consequences from its disruption, including diseases such as IBD. Our understanding of gastrointestinal physiology and pathogenesis has increased dramatically lately, but the translation of these findings to efficient therapeutics and associated biomarkers still lags behind. A significant reason for the latter is the limited availability of human cell systems that recapitulate cell interactions and functionality of the human tissue. The recent development of organoids, as patient-specific cell sources with unrestricted potential for propagation, has revolutionized our capabilities for experimentation with human cells. A major advantage of organoids is the potential to uncover a spectrum of disease phenotypes by direct comparisons between patient samples. A caveat of the system is that it cannot maintain the tissue microenvironment and cell–cell interactions critical for the identification of potential disease mechanisms for targeting.³⁹

Reproducible establishment of organoids from the small and the large intestine²⁵ is owing to the unique ability of the gut for lifelong renewal from the villous crypts. An important restriction of the organoids is that they do not allow for

Figure 3. (See previous page). The presence of stretch does not significantly contribute in the establishment of a tight epithelial barrier. (A) Representative phase-contrast images of the colonic epithelial on day 5 of the Colon Intestine-Chip culture in the presence or not of endothelium and/or stretch. (B) The P_{app} of the colonic epithelial cells to 3 kilodaltons of dextran Cascade blue, over the course of an 8-day culture, in the presence or absence of stretch (10% strain, 0.15 Hz) and/or endothelium. Stretch does not contribute significantly to the establishment of the epithelial barrier. Data shown correspond to 1 representative of 3 independent experiments. $n = 3$ –11 chips/condition, means \pm 95% CI, 2-way analysis of variance Tukey post hoc test. (C) Representative widefield fluorescent tile images showing the uniform expression of the TJ proteins, ZO-1 (green) and anti-E-cadherin (magenta), along the Colon Intestine-Chip (day 5) when endothelium is present. Cell nuclei are shown in blue. (D) Representative confocal immunofluorescence images indicating the basolateral localization of the transporter Na⁺K⁺ adenosine triphosphatase (ATPase) (magenta) and the apical localization of the transporter SLC26A3 (green) on day 5 of culture. Cell nuclei are shown in blue. The application of stretch does not affect the establishment of the polarity of the epithelial cells. The plots indicate the mean fluorescent intensity distribution for each channel, SLC26A3 (green) or Na⁺K⁺ATPase (magenta), along the basal–apical axis of the epithelial cells. The quantification was performed across 3 different fields of view in 3 individual chips for each condition. (E) Representative scanning electron microscopy (SEM) images of the colonic epithelial on day 5 of the Colon Intestine-Chip culture in the presence or not of endothelium and/or stretch, show the significant contribution of stretch on the maturation of the epithelial brush border only in the absence of endothelial cells. (F) Box plots showing the density of microvilli per μm^2 , according to quantification of SEM images on day 5 of culture, in the presence (top graph) and absence (bottom graph) of endothelium and/or stretch. The quantification was performed across 3–11 different fields of view for each condition. Each individual point represents a single field of view. Unpaired t test. * $P < .05$ and ** $P < .01$. DAPI, 4',6-diamidino-2-phenylindole.

direct access to the apical side of the cells, which face inward of the enclosed cystic cell structure.²⁵ This becomes a bottleneck in particular when mechanisms that drive epithelial barrier homeostasis are investigated because they

are linked to the strictly polarized expression of key proteins in the IECs. To address this need, methods for expansion of 3D organoids into monolayered epithelial structures were established in the Transwell culture



systems.^{40,41} These developments enabled studies with infectious agents, and co-culture of different cell populations, although in a nondynamic microenvironment. In the current study, we leveraged the developments in microphysiological systems and organoid technology to develop a human Colon platform for preclinical studies that incorporates critical aspects of the tissue microenvironment. We previously reported in a micro-engineered Duodenum Intestine-Chip the method for establishing a juxtaposed culture of human organoid-derived IECs and primary endothelium on tissue relevant-derived ECM.⁴² The microenvironment of the Colon Intestine-Chip includes shear stress and stretching to recapitulate aspects of the intestinal peristaltic motion. Although none of the stemness supporting factors is removed during the culture, unlike other protocols described previously^{25,43} we achieved a gradual differentiation of the organoid-derived IECs for the 8 days of culture. Furthermore, the presence of endothelium from the beginning of the culture was found to support the earlier establishment of a tight epithelial barrier, a consistent finding in all donors tested and aligned with former studies using a duodenum-based Intestine-Chip.¹³ As described earlier, up-regulation of key signaling pathways related to epithelial differentiation, metabolism, and ion transportation unveil the physiological relevance of the transcriptomic phenotype of the Colon Intestine-Chip. The robustness and reproducibility of the protocol and the demonstrated interindividual variability in the pace of differentiation of colonoids to epithelial cell subtypes were highly suggestive of the potential of the Colon Intestine-Chip as a platform for human studies. For further confirmation of the latter, we proceeded with an assessment of the functional response of the Colon Intestine-Chip to a well-established barrier disruption cytokine, IFN γ .⁷ As has been shown by studies with cell lines and *in vivo* experimental models, IFN γ modulates the integrity of both the intestinal epithelial⁷ and endothelial⁴⁴ barriers. Disruption of the epithelial barrier, specifically, is driven by apoptosis²⁸ and cytoskeletal remodeling, via up-

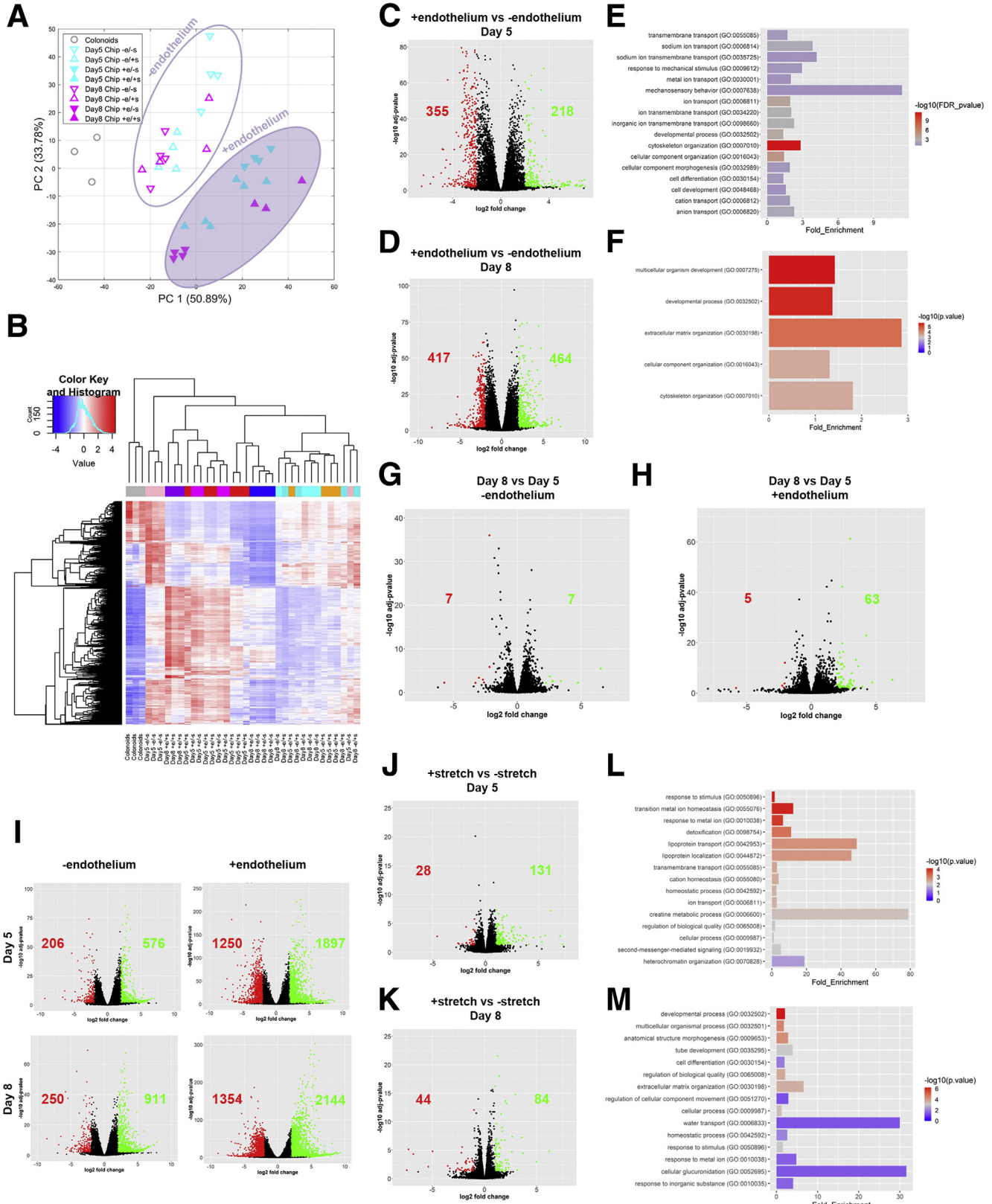
regulation of MLCK.⁵ We found that upon exposure to IFN γ , the Colon Intestine-Chip showed loss of the epithelial barrier integrity in a concentration- and time-dependent manner reproduced in all donors used in this study. Activation of apoptosis, as indicated by the cleavage of caspase 3, and erosion of the epithelial TJ were detected as early as 48 hours after stimulation in comparison with previously described models using T84 and Caco2 monolayers.^{7,28,45} These results indicate the response and sensitivity of the Colon Intestine-Chip platform to a well-established, disease-relevant, barrier-disruption bioassay and provide reassurance for its potential to complement and further advance existing models.

Next, we applied the Colon Intestine-Chip to elucidate the effect of IL22, a member of the IL10 family of cytokines secreted in human beings primarily by subpopulations of CD4⁺ T cells, including T_h22, T_h17, T_h1, and $\gamma\delta$ T cells, as well as innate lymphoid cell 3, natural killer cells, and dendritic cells.^{31,46-48} Increased levels of IL22 have been detected in the intestinal mucosa of IBD and the serum of Crohn's disease patients.⁴⁹ Although several reports advocated for a protective role of IL22 in the inflammatory state because it promotes cell survival and proliferation as well as secretion of mucins, chemokines, and antimicrobial peptides of the S100 and Regenerative Genes families,⁵⁰⁻⁵² the overall effects of IL22 in the epithelial barrier homeostasis, as per animal and human studies, remain unclear.^{53,54} Our findings in the Colon Intestine-Chip showed a concentration-dependent increase of epithelial permeability in response to IL22, consistent with studies in Transwells with Caco2 cells,¹⁸ although they do not support its regenerative effect on the crypt stem cells, as described in murine experimental models.³⁷ This observation could be linked to the low representation of proliferating cells at the time of IL22 administration in our platform and suggest a differential effect of the cytokine on differentiated enterocytes. IL22 acts via activation of STAT3 and STAT1. It has been hypothesized that the cross-talk between type I IFNs and

Figure 4. (See previous page). Endothelium supports the establishment of a tight epithelial barrier over the course of the culture. (A) Representative confocal fluorescent images showing the establishment of strong epithelial TJs on day 8 of the culture in the presence of endothelium. TJs were stained with anti-ZO-1 and anti-E-cadherin and cytoskeleton with phalloidin (gray). Cell nuclei are shown in blue. (B) Representative confocal immunofluorescence images, against the basolateral transporter Na⁺K⁺ adenosine triphosphatase (ATPase) (magenta) and the apical transporter SLC26A3 (green), indicating the establishment of a polarized epithelial monolayer only during the co-culture of colonocytes with endothelium, on day 8 of culture. Cell nuclei are shown in blue. The plots indicate the mean fluorescent intensity distribution for each channel along the basal-apical axis of the epithelial cells. The quantification was performed across 3 different fields of view in 3 individual chips for each condition. (C) The gene expression of the 2 epithelial junction proteins, *Cdh1* and *Tjp1*, was confirmed in epithelial cells on days 5 and 8 of culture of the Colon Intestine-Chip. The on-chip culture enhances the expression of both proteins. The graph represents fragments per kilobase of transcript per million mapped reads (FPKM) values generated from bulk RNA-seq analysis of the epithelial cells and plotted on a box plot, where each individual point represents a single chip. n = 3-6 chips/condition, means \pm 95% CI, 1-way analysis of variance, Tukey post hoc test. (D) The gene expression of the 2 ion transporters, *Atp1a1* and *Slc26a3*, was confirmed in epithelial cells on days 5 and 8 of culture of the Colon Intestine-Chip. The on-chip culture enhances the expression of both transporters. The graph represents FPKM values generated from bulk RNA-seq analysis of the epithelial cells and plotted on a box plot, where each individual point represents a single chip. n = 3-6 chips/condition, means \pm 95% CI, 1-way analysis of variance, Tukey post hoc test. (E) Representative scanning electron microscopy (SEM) images of the colonic epithelial on day 8 of the Colon Intestine-Chip culture, where stretch (10% strain, 0.15 Hz) is applied in the presence or not of endothelium. Endothelium does not significantly contribute to the establishment of a dense microvilli network at a later stage of the culture. (F) Box plots showing the density of microvilli per μm^2 , according to quantification of SEM images on day 8 of culture. The quantification was performed across 8-9 different fields of view for each condition. Each individual point represents a single field of view. Unpaired t test. **P* < .05, ***P* < .01, ****P* < .001, and *****P* < .0001. DAPI, 4',6-diamidino-2-phenylindole.

the members of the IL10 cytokine family, IL10 and IL22, may alter the downstream pathway landscape by enhancing a STAT1-mediated proinflammatory response.^{55,56}

Moreover, recent reports have indicated an IL22-elicited inhibition of Wnt and Notch pathways in small intestinal organoids, limiting the renewal of the leucine-rich repeat-



containing G-protein-coupled receptor 5-positive stem cell pool.³⁵ These data collectively suggest a biological action of IL22 dependent on the specific characteristics of the experimental model used and further support the detrimental effect of IL22 during a time window during which few self-renewing stem cells still are present. Independent of its short-term effects, prolonged exposure to IL22 has been associated with chronic diseases such as intestinal inflammation and cancer.^{57,58} Additional complexity is added by secretion of IL22BP, which binds the cytokine with higher affinity than the transmembrane receptor⁵⁹ and modulates the threshold of its action on intestinal epithelium. Even if accumulating evidence suggests a pathophysiological role of IL22BP in experimental colitis, the different cell source and levels of expression among rodents and human beings still provide room to elucidate the role of IL22BP in the progression of the human disease.⁶⁰ Blockade of the IL22 effect on STAT3 activation and loss of the epithelial barrier integrity by co-treatment of the Colon Intestine-Chip with IL22BP shows the specificity of the effect. Moreover, it suggests that this platform can be used to decipher species-specific discrepancies in the mechanism of action of multifaceted cytokines. Investigation of the potential compensatory actions of IL22 in the inflamed epithelium is beyond the scope of this study.

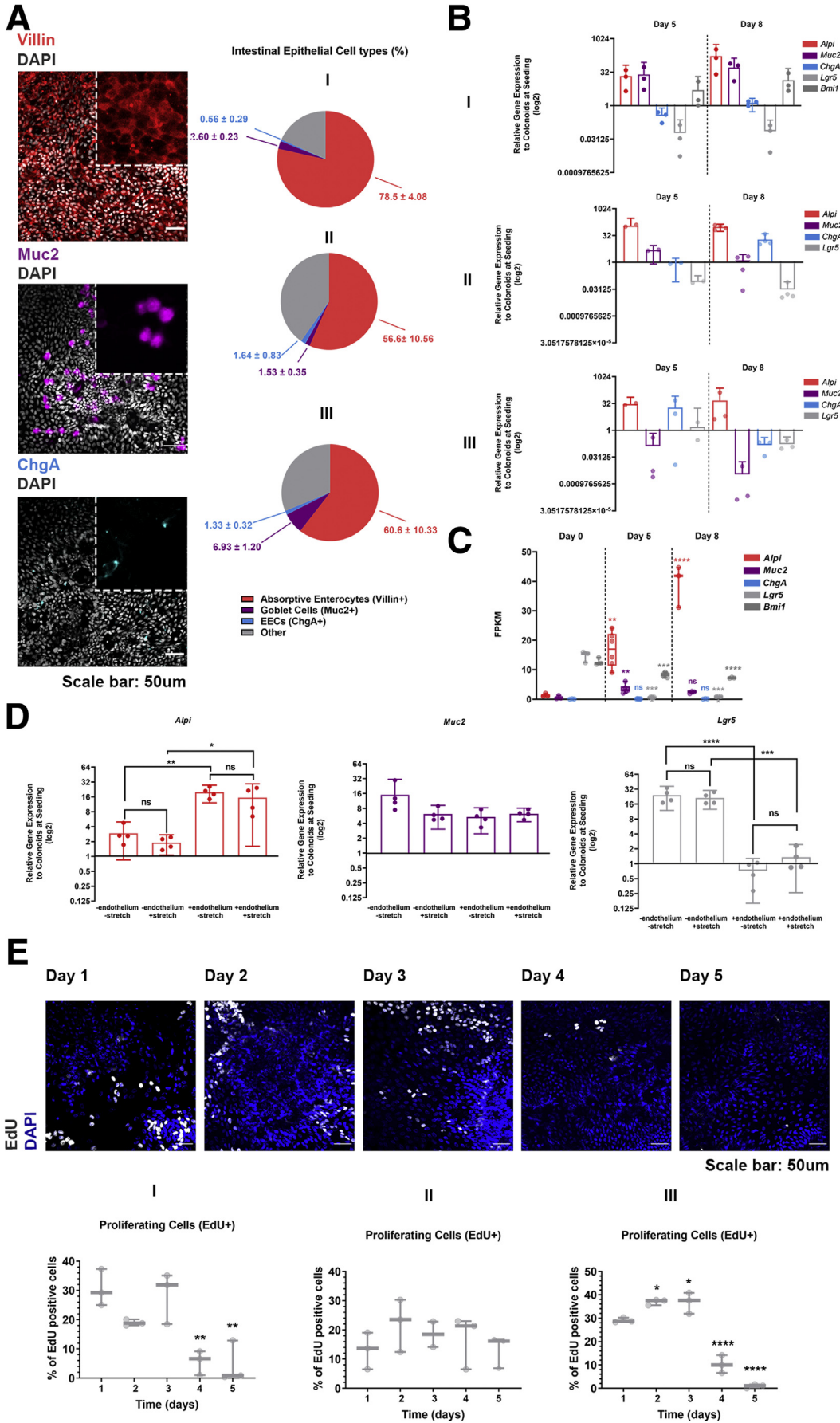
In summary, we report here the development of a Colon Intestine-Chip, a microphysiological system that provides the microenvironment to enable differentiation of human organoids to an epithelial monolayer of polarized cells forming a tight barrier. We show that this human platform can be used to study potential barrier-disruptive factors in a reproducible and specific manner. The implications of these findings for understanding the regulation of barrier function are very important given the list of conditions causing leaky barrier and the association of the latter with degenerative and other diseases. It is not lost on us that this system ultimately can be used to study biology beyond barrier function including the functionality of novel proteins in different cell types represented in the system via genetic manipulation systems such as clustered regularly interspaced short palindromic repeats (CRISPR).

Materials and Methods

Cell Culture

Human biopsy-derived colonoids, from 2 male donors and 1 female donor, isolated according to experimental protocols approved by Johns Hopkins University Institutional Review Board (NA_00038329), were provided by Professor Mark Donowitz's research group.

Figure 5. (See previous page). On-Chip culture enhances biological processes related to the maturation of the intestinal epithelium. (A) Principal component analysis shows that the presence of endothelium clearly separates the epithelial transcriptome of the Chips cultured with and without endothelium. (B) Heatmap representation of the 1000 most variant genes. Samples cultured in the presence of endothelium are clustered separately from all other conditions. (C) The volcano plot resulting from the differential gene expression analysis between the epithelial cells on day 5 of culture, where stretch (10% strain, 0.15 Hz) is applied in the presence and absence of endothelium. The number of the up-regulated and down-regulated differentially expressed genes in the presence of endothelium is shown in green and red, respectively. (D) The volcano plot resulting from the differential gene expression analysis between the epithelial cells on day 8 of culture, where stretch (10% strain, 0.15 Hz) is applied in the presence and absence of endothelium. The number of the up-regulated and down-regulated genes in the presence of endothelium is shown as green and red, respectively. (E) List of biological processes identified by the GO enrichment analysis using the differentially expressed genes between the epithelial cells on day 5 of culture, where stretch (10% strain, 0.15 Hz) is applied in the presence and absence of endothelium. The results indicate the significant enrichment of biological processes related to the morphogenesis and function of the epithelial barrier. (F) List of biological processes identified by the GO enrichment analysis, using the differentially expressed genes between the epithelial cells on day 8 of culture, where stretch (10% strain, 0.15 Hz) is applied in the presence and absence of endothelium. The results indicate significant enrichment of biological processes related to the morphogenesis of the epithelial barrier. (G) The volcano plot resulting from the differential gene expression analysis between the epithelial cells cultured in the absence of endothelium and the presence of stretch (10% strain, 0.15 Hz), on days 5 and 8 of culture. The number of up-regulated and down-regulated genes at the end of the culture is shown in green and red, respectively. (H) The volcano plot resulting from the differential gene expression analysis between the epithelial cells cultured in the presence of endothelium and stretch (10% strain, 0.15 Hz), on days 5 and 8 of culture. The number of the up-regulated and down-regulated genes at the end of the culture is shown in green and red, respectively. $n = 3-6$ chips/condition. (I) The volcano plots resulting from the differential gene expression analysis between the epithelial cells cultured on chip on days 5 and 8, with the presence of stretch (10% strain, 0.15 Hz) and the presence or absence of endothelium and colonoids. The number of the up-regulated and down-regulated differentially expressed genes in chips is shown in green and red, respectively. (J) The volcano plot of the differential gene expression analysis between the epithelial cells on day 5 of culture with endothelium, in the presence and absence of stretch (10% strain, 0.15 Hz). The number of the up-regulated and down-regulated differentially expressed genes in the presence of stretch is shown in green and red, respectively. (K) The volcano plot resulting from the differential gene expression analysis between the epithelial cells on day 8 of culture with endothelium, in the presence and absence of stretch (10% strain, 0.15 Hz). The number of the up-regulated and down-regulated differentially expressed genes in the presence of stretch is shown in green and red, respectively. (L) List of biological processes identified by the GO enrichment analysis, using the differentially expressed genes between the epithelial cells on day 5 of culture with endothelium, in the presence and absence of stretch (10% strain, 0.15 Hz). The results indicate the significant enrichment of biological processes related to the homeostasis and function of the epithelial barrier. (M) List of biological processes identified by the GO enrichment analysis, using the differentially expressed genes between the epithelial cells on day 8 of culture with endothelium, in the presence and absence of stretch (10% strain, 0.15 Hz). The results indicate the significant enrichment of biological processes related to the morphogenesis, function, and homeostasis of the epithelial barrier. $n = 3-6$ chips/condition.



Colonoids were cultured in Matrigel (356231; Corning, Corning, NY) and in the presence of the commercially available medium IntestiCult Organoid Growth Medium (human) (06010; STEMCELL Technologies, Vancouver, Canada), supplemented with the antibiotic primocin (ant-pm-2; Invivogen, San Diego, CA) in a concentration of 1:500 (vol/vol). Passaging was performed every 7 days, colonoids were recovered from the Matrigel using Cell Recovery Solution (cat. no. 354253; Corning), and fragmented for 2 minutes at 37°C in a digestion solution containing TrypLE (12604013; Thermo Fisher Scientific, Waltham, MA), diluted with phosphate-buffered saline (PBS) 1 × 1:1 (vol/vol), and supplemented with 10 μmol/L Y-27632. Both 10 μmol/L Y-27632 (Y0503; Sigma-Aldrich, St. Louis, MO) and 5 μmol/L CHIR99021 (04-0004-10; Stemgent, Cambridge, MA) were present in the culture medium for 72 hours after passaging.

Colonic human intestinal microvascular endothelial cells (cHIMECs) were obtained from Cell Biologics (H-6203; Chicago, IL) and Cell Systems (ACBRI 666; Kirkland, WA). cHIMECs were cultured in gelatin-coated (6950; Cell Biologics) flasks in endothelial cell growth medium MV2 (C-22121; Promo Cell, Heidelberg, Germany), which contained 5 ng/mL recombinant human epidermal growth factor, 10 ng/mL recombinant human basic fibroblast growth factor, 20 ng/mL R3 insulin-like growth factor, 0.5 ng/mL recombinant human vascular endothelial growth factor, 1 μg/mL ascorbic acid, 0.2 μg/mL hydrocortisone, 5% fetal bovine serum (F4135; Sigma-Aldrich), and 1:1000 (vol/vol) primocin.

Cells were cultured in a humidified environment at 37°C in 5% CO₂. For the experiment, human colonoids of passage 30 or earlier, and cHIMECs of passage 7 or below, were used.

Establishment of the Colon Intestine-Chip

The Colon Intestine-Chip (10231-2; Emulate, Inc) consists of 2 parallel channels separated by a porous polydimethylsiloxane (PDMS) membrane (diameter, 7 μm; spacing, 40 μm; thickness, 50 μm), and 2 lateral channels where vacuum is applied. The dimensions of the top channel, where colonic epithelial cells reside, are 1000 × 1000 μm (width × height), its volume is 28.041 μL, and its cell culture surface is 28 mm². The endothelial cells were introduced in the bottom channel, the dimensions of which are 1000 × 200 μm (width × height), its volume is 5.584 μL, and its cell culture surface is 24.5 mm². The interface of the 2 cell types extended in an area of 17.1 mm². The timeline of the establishment of the Colon Intestine-Chips was as follows (Figure 1).

Day -1. The PDMS membrane was activated using Emulate Reagent 1 (ER1) and Emulate Reagent 2 (ER2) reagents (10465; Emulate). A solution of 0.5 mg/mL ER1 in ER2 was prepared and 50 μL was introduced in each channel. Chips were incubated under UV light for 10 minutes, followed by 3 minutes of incubation at room temperature and another 10 minutes of UV treatment. Subsequently, both channels were washed with ER2, then PBS 1 ×, and coated overnight at 37°C, with 200 μg/mL collagen IV (C5533; Sigma-Aldrich) and 100 μg/mL Matrigel (Corning), and 200 μg/mL collagen IV (Sigma-Aldrich) and 30 μg/mL fibronectin (356008; Corning), in the top and bottom channels, respectively.

Day 0. To be seeded on the Chips, colonoids were recovered from Matrigel using Cell Recovery Solution (Corning), and fragmented by incubation at 37°C for 2 minutes in a digestion solution containing TrypLE (Thermo Fisher Scientific), diluted with PBS 1 × 1:1 (vol/

Figure 6. (See previous page). (See previous page) On-Chip culture supports the multilineage differentiation of the colonic epithelial cells. (A) Representative confocal fluorescent images showing the presence of absorptive enterocytes (anti-villin, red), Goblet cells (anti-mucin 2, magenta), and enteroendocrine cells (anti-ChgA, cyan) on day 8 of culture. Cell nuclei are shown in gray. The pie charts plot the percentage of the respective cell types for each of the 3 different donors. The total number of cells is evaluated based on 4',6-diamidino-2-phenylindole (DAPI) staining. The quantification was performed across 5 different fields of view in 3 individual chips for each cell type and donor. Means ± SD. (B) Identification of each epithelial cell type by qPCR for the *Alpi*, *Muc2*, *ChgA*, *Lgr5*, and *Bmi1* genes. The relative gene expression values of each gene at the respective time points (day 5 and day 8) are normalized to colonoids at seeding. 18S has been acquired as the housekeeping gene. The expression of indicative for the mature enterocytes and quiescent stem cells genes increase over the course of the culture whereas the expression of the cycling stem cells driving gene *Lgr5* decreases. A donor-dependent expression was observed for the mature enterocytes and cycling stem cells driving genes. Each individual spot represents a single chip. n = 2–4 chips/day, means ± 95% CI. (C) The gene expression of *Alpi*, *Muc2*, *ChgA*, and *Lgr5* on days 0, 5, and 8 of culture of donor I. The expression of indicative for the mature absorptive enterocytes and Goblet cell genes increases over the course of the culture, whereas the expression of the cycling stem cells driving gene *Lgr5* and of the quiescent stem cell gene *Bmi1* decreases. Fragments per kilobase of transcript per million mapped reads (FPKM) values generated from bulk RNA-seq analysis of the epithelial cells are plotted on a box plot, where each individual point represents a single chip n = 3–6 chips/condition, 1-way analysis of variance, Tukey post hoc test. (D) Identification of each epithelial cell type by qPCR for *Alpi*, *Muc2*, *ChgA*, and *Lgr5* on day 5 of culture in the presence of stretch and/or endothelium. Endothelium significantly enhances the gene expression of the absorptive enterocyte marker *Alpi* and decreases the expression of the cycling stem cells driving gene *Lgr5*. Each individual spot represents a single chip. n = 4 chips/condition, means ± 95% CI, 1-way analysis of variance, Tukey post hoc test. n = 2–4 chips/day for each donor, means ± 95% CI. (E) Confocal fluorescent images of 3 different donors indicating the abundance of proliferating cells (EdU, gray) over the course of the first 5 days of culture. Cell nuclei are shown in blue. The total number of cells is evaluated based on DAPI staining and the percentage of the EdU-positive cells is shown on a box plot, where each individual dot represents a single chip. The quantification was performed across 3 different fields of view in 3 individual chips for each day of the culture and donor. The abundance of the proliferating cells was decreased significantly on days 4 and 5 of the culture. One-way analysis of variance, Tukey post hoc test. *P < .05, **P < .01, ***P < .001, and ****P < .0001.

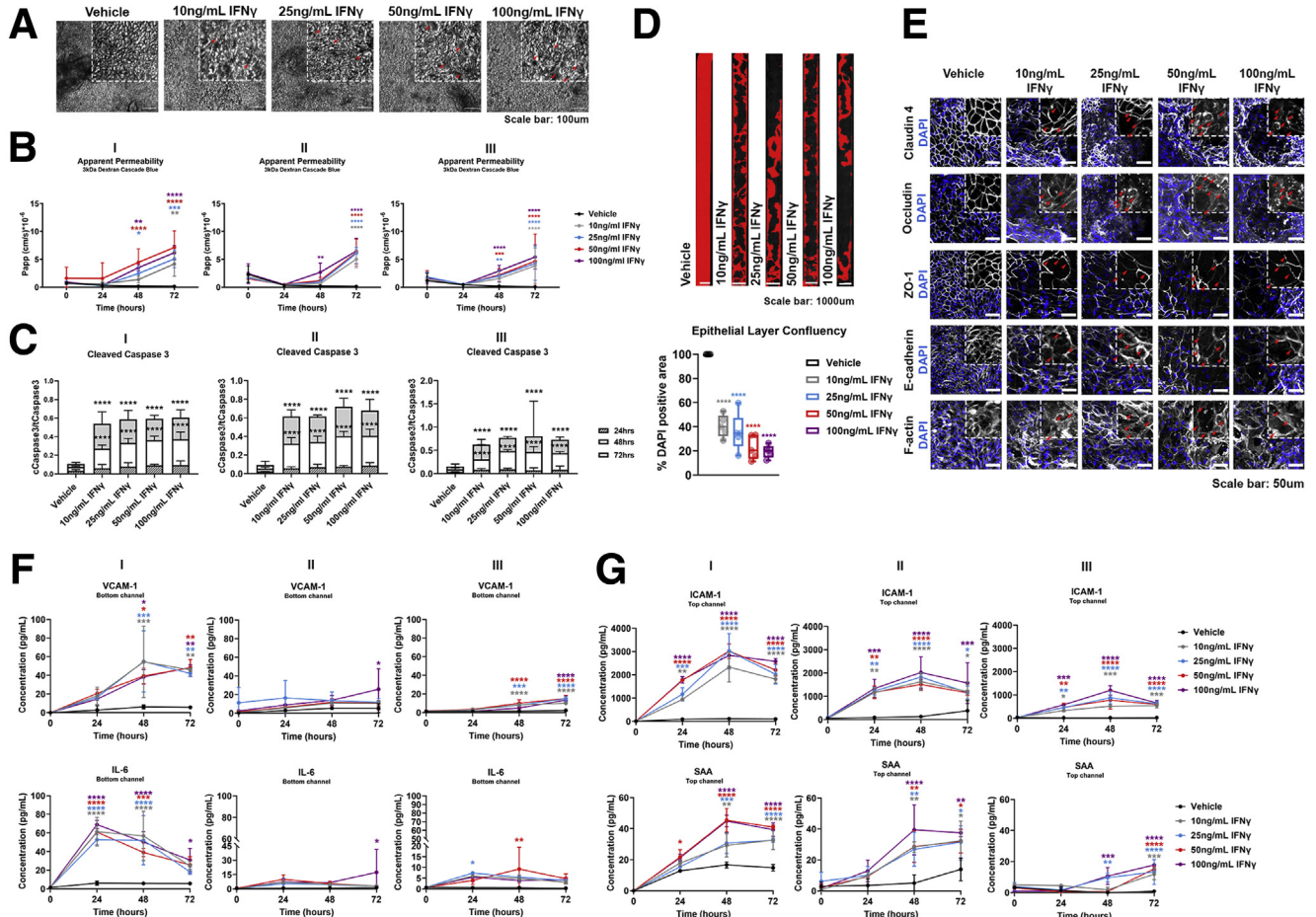
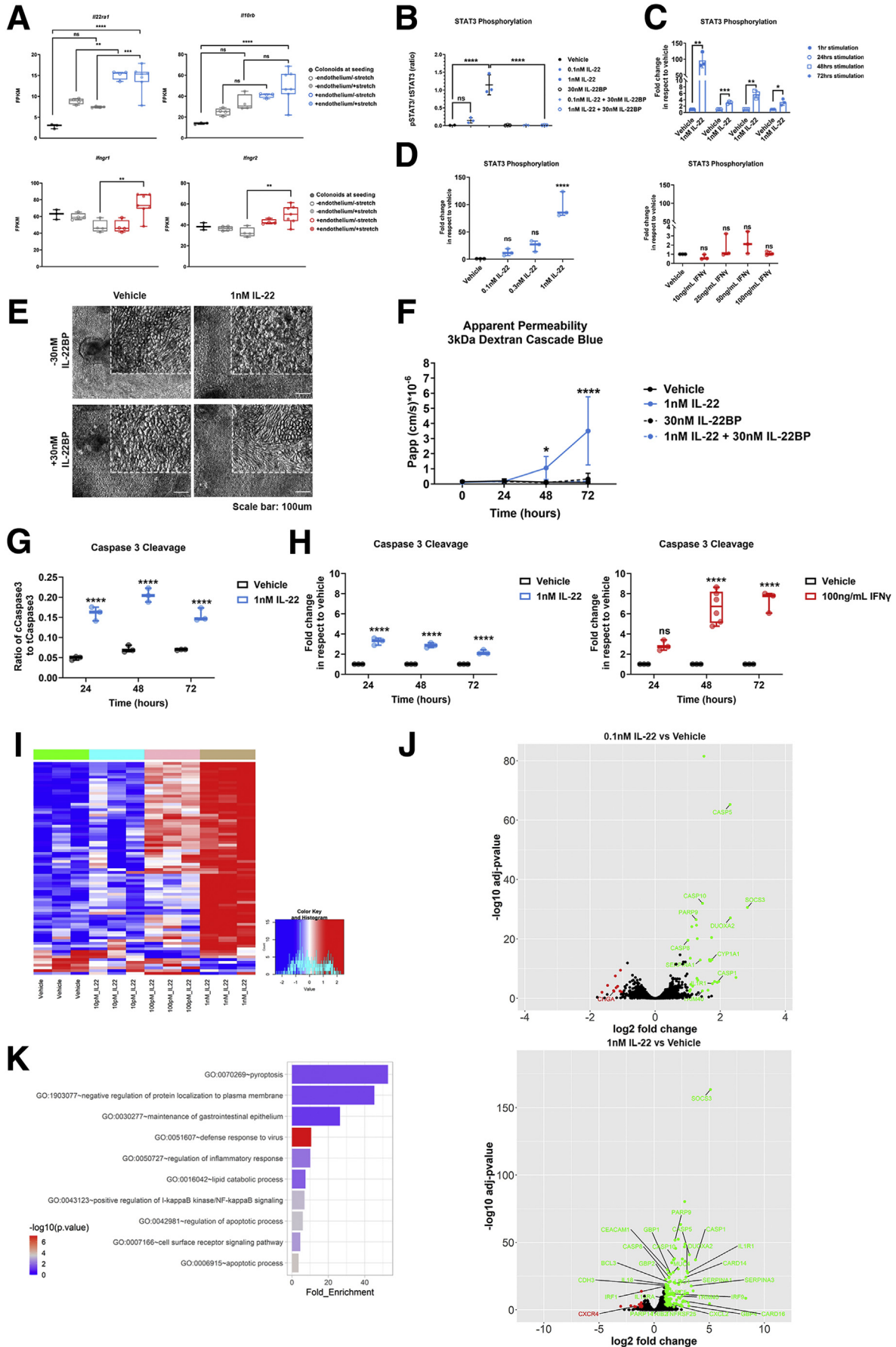


Figure 7. The established epithelial barrier responds in a time- and concentration-dependent manner to IFN γ , a barrier-disruptive agent. (A) Representative phase-contrast images of the colonic epithelial monolayer 48 hours after treatment with IFN γ . Gradual degeneration of the morphology of the epithelial cells was observed as the concentration of IFN γ increased, indicating a transition from columnar to the squamous-shaped epithelium (*red arrows*). (B) The P_{app} of epithelial cells to 3 kilodaltons dextran Cascade blue, over the course of 72 hours of basolateral stimulation with IFN γ , indicates a dose-, donor-, and time-dependent barrier disruption. Data shown correspond to 1 representative of 3 independent experiments. $n = 3$ –12 chips/condition, means \pm 95% CI, 2-way analysis of variance, Tukey post hoc test. (C) Quantification of the cleaved over total caspase 3 in epithelial cells shows a significant and concentration-dependent activation of apoptosis 48 and 72 hours after stimulation across 3 different donors. $n = 3$ chips/condition means \pm 95% CI, 2-way analysis of variance, Tukey post hoc test. (D) Representative tile fluorescent images highlighting the area of the Colon Intestine-Chip covered with epithelial cells, determined by positive 4',6-diamidino-2-phenylindole (DAPI) staining (*red*), 48 hours after stimulation with different concentrations of IFN γ . The epithelial layer confluency is expressed as a percentage of the DAPI-positive area over the total area of the chip, depicted as a box plot where each individual point represents a single chip. A significant and concentration-dependent decrease of the epithelial layer confluency was observed 48 hours after treatment with IFN γ . $n = 4$ –5 chips/condition, means \pm 95% CI, 1-way analysis of variance, Tukey post hoc test. (E) Representative confocal immunofluorescence images indicating the dose-dependent degeneration of the epithelial TJs, as shown by the redistribution of claudin 4, ZO-1, and F-actin, and internalization of occludin and E-cadherin (*red arrows*). Cell nuclei are shown in blue. (F) Time-course quantification of cytokines and vascular injury-related serum proteins in the Colon Intestine-Chip shows a concentration-, donor-, and time-dependent secretion of IL6 and vascular cell adhesion molecule-1 (VCAM-1) in the bottom channel, upon treatment with IFN γ . $n = 3$ chips/condition, means \pm SD, 2-way analysis of variance, Tukey post hoc test. (G) Time-course quantification of vascular injury-related serum proteins in the Colon Intestine-Chip shows a concentration-, donor-, and time-dependent secretion of intercellular cell adhesion molecule-1 (ICAM-1) and serum amyloid A (SAA) in the top channel, upon treatment with IFN γ . $n = 3$ chips/condition, means \pm SD, 2-way analysis of variance, Tukey post hoc test. * $P < .05$, ** $P < .01$, *** $P < .001$, and **** $P < .0001$.

vol) and supplemented with 10 μ mol/L Y-27632. They were resuspended in IntestiCult medium, supplemented with 10 μ M Y-27632 (Sigma-Aldrich) and 5 μ M CHIR99021 (Stemgent), and introduced in the apical

channel of the Colon Intestine-Chip in a seeding density of 7×10^6 cells/mL. To assess the cell density, part of the seeding cell suspension was incubated in ACCUTASE (07920; STEMCELL Technologies) for 30 minutes and



fragmented to a single-cell level. Both 10 $\mu\text{mol/L}$ Y-27632 and 5 $\mu\text{mol/L}$ CHIR99021 were maintained in the culture medium for 72 hours thereafter.

When investigating the interaction between epithelial and endothelial cells, cHIMECs were seeded on the basal side of the PDMS membrane 1 hour before the seeding of epithelial cells in the top channel. Briefly, 20 μL of the suspension of endothelial cells, in a seeding density of 8×10^6 cells/mL, were introduced in the bottom channel, and Colon Intestine-Chips were incubated inverted at 37°C, in a humidified environment. The bottom channel was washed and thereafter immersed in endothelial cell growth medium MV2 medium.

Day 1. Both channels were washed with the corresponding media to remove the nonadherent cells. Colon Intestine-Chips were attached to devices called Pod Portable Modules (10153; Emulate, Inc) and connected in the automated cell culture system Zoë Culture Module (Emulate, Inc). Each Zoë is connected to an Orb Hub module that supplies the gas, vacuum, and power. The flow rate was set at 60 $\mu\text{L/h}$ in both channels.

Day 2. Medium without Y-27632 and CHIR99021 was replenished in both channels.

Day 3. Colon Intestine-Chips were acclimated to mechanical forces using 2% strain and 0.15-Hz frequency.

Day 4. Stretching was increased to 10% strain and 0.15-Hz frequency, and culture medium was replenished. Both

channels were perfused at 1000 $\mu\text{L/h}$ for 5 minutes to flush out any detached cells.

Days 5–8. Culture media was refreshed, and detached cells were removed by flushing (1000 $\mu\text{L/h}$, 5 min) every other day of the culture.

Assessment of Apparent Permeability

The epithelial barrier integrity was assessed based on the apparent permeability of 3 kilodaltons of dextran Cascade Blue molecule (100 $\mu\text{g/mL}$, D7132; Thermo Fisher), applied in the medium of the top channel of the Colon Intestine-Chip. The diffusion of the dye to the bottom channel was monitored based on a standard curve and the absorbance of the bottom channel effluents at 375–420 nm. For the calculation of the P_{app} , the following mathematical formula was used:

$$P_{\text{app}} = \frac{V_{\text{rec}} \cdot dC_{\text{rec}}}{A \cdot dt \cdot C_{\text{don}, t=0}}$$

Where P_{app} is the apparent permeability (cm/s), V_{rec} is the volume of the retrieved effluent from the bottom channel (mL), dC_{rec} is the difference of the concentration of the dye in the effluent and input medium of the bottom channel (mg/mL), A is the surface area on which the diffusion of the dye occurs (cm²), dt is the time period on which the P_{app} is assessed (s), and $C_{\text{don}, t=0}$ is the concentration of the dye in the dosing epithelial medium (mg/mL).

Figure 8. (See previous page). IL22 induces disruption of the epithelial barrier in the Colon Intestine-Chip, an effect rescued by the presence of its soluble receptor IL22BP. (A) The gene expression of the 2 subunits of the transmembrane IL22 receptor, *Il22ra1* and *Il10rb*, and IFN γ receptor, *Ifngr1* and *Ifngr2*, was confirmed in epithelial cells on day 5 of culture of the Colon Intestine-Chip. The on-chip culture enhances the expression of both receptors. Fragments per kilobase of transcript per million mapped reads (FPKM) values generated from bulk RNA-seq analysis of the epithelial cells are plotted on a box plot, where each individual point represents a single chip. $n = 3\text{--}6$ chips/condition, 1-way analysis of variance, Tukey post hoc test. (B) Quantification of the phosphorylated over the total STAT3 in epithelial cells of the Colon Intestine-Chip, shows a concentration-dependent activation of STAT3 1 hour after stimulation with 0.1 or 1 nmol/L IL22. In the presence of IL22BP the activation of STAT3 is negated. $n = 3$ chips/condition means \pm SD, 1-way analysis of variance, Tukey post hoc test. (C) Quantification of the phosphorylated over the total STAT3 in epithelial cells of the Colon Intestine-Chip, expressed as fold increase over the vehicle, shows a sustained activation of STAT3 over the course of 72 hours of stimulation with 1 nmol/L IL22. $n = 3$ chips/condition means \pm SD, unpaired t test performed for each time point. (D) Quantification of the phosphorylated over the total STAT3 in epithelial cells of the Colon Intestine-Chip, expressed as fold increase over the vehicle, shows a cytokine-specific activation of STAT3 upon stimulation with various concentrations of IL22 and IFN γ . Each individual point in the box plot represents a single chip. $n = 3$ chips/condition, 1-way analysis of variance, Tukey post hoc test. (E) Representative phase-contrast images of the colonic epithelial monolayer 48 hours after treatment with 1 nmol/L IL22, shows a compromised morphology of the epithelial cells. The epithelial cell morphology is rescued in the presence of 30 nmol/L IL22BP. (F) The P_{app} of epithelial cells to 3 kilodaltons dextran Cascade blue, over the course of 72 hours of stimulation with 1 nmol/L IL22 and/or 30 nmol/L IL22BP. IL22 triggers loss of the epithelial barrier integrity, which is rescued upon co-treatment with IL22BP. $n = 3\text{--}6$ chips/condition, means \pm 95% CI, 2-way analysis of variance, Tukey post hoc test. (G) Quantification of the cleaved over the total caspase 3 in epithelial cells of the Colon Intestine-Chip, indicates a significant and sustained increase in the levels of activated caspase 3 over the course of 72 hours of stimulation with 1 nmol/L IL22. Each individual point in the box plot represents a single chip. $n = 3$ chips/condition, 2-way analysis of variance, Tukey post hoc test. (H) Quantification of the cleaved over the total caspase 3 in epithelial cells of the Colon Intestine-Chip, expressed as fold increase over the vehicle, shows a cytokine- and time-dependent activation of apoptosis over the course of 72 hours of stimulation with either 1 nmol/L IL22 or 100 ng/mL IFN γ . Each individual point in the box plot represents a single chip. $n = 3\text{--}6$ chips/condition, 2-way analysis of variance, Tukey post hoc test. (I) Heatmap of the 1000 most variant genes across samples cultured in the presence of different conditions (ie, vehicle and 3 different concentrations of IL22). $n = 3$ chips/condition. (J) The volcano plot resulting from the differential gene expression analysis between the epithelial cells on day 5 of culture under baseline conditions and upon stimulation with 0.1 or 1 nmol/L IL22. Genes up-regulated and down-regulated in the presence of IL22 are shown in green and red, respectively. (K) List of biological processes identified by the Gene Ontology enrichment analysis, using the differentially expressed genes between the epithelial cells on day 5 of culture under baseline conditions and upon stimulation with 1 nmol/L IL22. The results indicate significant enrichment of biological processes related to the inflammatory response and apoptotic pathway in the presence of IL22. * $P < .05$, ** $P < .01$, *** $P < .001$, and **** $P < .0001$.

Table 1. List of Antibodies Used in Immunofluorescence

Target epitope	Host species	Vendor	Catalog number	Dilution ratio
Mucin 2	ms	Santa Cruz Biotechnology	sc- 515032	1:300
Villin	rb	Abcam	ab130751	1:100
Chromogranin A	rb	Abcam	ab15160	1:100
ZO-1	ms	Thermo Fischer	339194	1:100
E-cadherin	ms	Abcam	ab1416	1:100
Occludin	ms	Thermo Fischer	33-1500	1:100
Claudin 4	rb	Thermo Fischer	36-4800	1:100
Na ⁺ K ⁺ adenosine triphosphatase	ms	Abcam	ab7671	1:100
SLC26A3	rb	Abcam	ab244452	1:100

ms, mouse; rb, rabbit.

Cytokine Stimulation

IL22 (782-IL-010; R&D, Minneapolis, MN), in the presence or absence of 30 nmol/L IL22BP (8498-BP-025; R&D) and IFN γ (300-02; Peprotech, Rocky Hill, NJ) was introduced in the culture medium of the endothelial channel at various concentrations. The cytokine-supplemented medium was refreshed every 24 hours and the appropriate vehicle controls were used in each stimulation experiment.

Immunofluorescence

At the indicated time points Colon Intestine-Chips were fixed at room temperature for 15 minutes in 4% paraformaldehyde solution, or at -20°C for 20 minutes in ice-cold methanol according to the target epitope. Briefly, chips were washed in both channels with PBS 1 \times , immersed in permeabilization solution (10% normal donkey serum, 0.1% Triton X-100 in PBS 1 \times) for 15–30 minutes at room temperature followed by blocking solution (10% NDS in PBS 1X) for 1 hour, and incubated with primary antibody (Table 1), overnight at 4°C. Subsequently, chips were stained with the appropriate combination of secondary Alexa Fluor antibodies (Abcam, Cambridge, MA) and counterstained with 50 μ g/mL 4',6-diamidino-2-phenylindole (D1306; Invitrogen, Carlsbad, CA). The antibody solutions were prepared using 5% normal donkey serum in PBS 1 \times in the dilution ratios mentioned in Table 1. In the case of morphologic analysis of the epithelial cytoarchitecture, F-actin was stained with phalloidin, conjugated with the appropriate Alexa Fluorophores (Abcam), added in the secondary antibody solution. To assess epithelial cell proliferative capacity,

epithelial cells in the chips were treated with 20 μ mol/L, harvested 24 hours later, and EdU reactivity was assessed as per the manufacturer's instructions (C10337; Thermo Fisher).

Assessment of ECM Coating

ECM proteins were stained using an Alexa Fluor 488-conjugated NHS ester (A20100; Thermo Fisher). After membrane activation and coating, each channel was pre-treated with borate buffer (pH 8.5) at room temperature for 5 minutes and stained with NHS ester dye solution in borate buffer (1:500) at room temperature for 25 minutes in the dark. Both channels were rinsed gently with PBS 1 \times before and images were acquired.

Imaging and Imaging Quantification

Phase-contrast images were acquired using the Zeiss (Peabody, MA) AXIOvert.A1 brightfield microscope (objective: Zeiss LD A-Plan 10 \times /0.25 Ph1) and the Zeiss Axiocam 503 mono camera. Fluorescent z-stack images and fluorescent tile images of the Colon Intestine-Chip were acquired using the inverted laser-scanning confocal microscope Zeiss LSM 880 (objective: Zeiss LD Plan-Neofluar 20 \times /0.40 Korr M27), and the epifluorescence inverted microscope Olympus (Waltham, MA) IX83 (objective: Olympus CPlanFL N 10 \times /0.30 RC1) and the Hamamatsu (Boston, MA) ORCA Flash 4.0 camera, respectively. Image processing and quantification were performed using Fiji (version 2.0, NIH, Bethesda MD), as per standard methods.

Table 2. List of Human TaqMan Gene Expression Assays Used in qRT-PCR

Gene ID	Gene name	TaqMan assay ID
18S	18S ribosomal RNA	Hs99999901_s1
Alpi	Alkaline phosphatase intestinal	Hs00357579_g1
Muc2	Mucin 2	Hs00894025_m1
Chga	Chromogranin A	Hs00900375_m1
Lgr5	Leucine-rich-repeat-containing G-protein-coupled receptor 5	Hs00969422_m1
Bmi1	Polycomb complex protein BMI-1	Hs00409825_g1

Table 3. List of Epithelial Cell Samples Isolated at Different Conditions and Time Points of the Colon Intestine-Chip Culture, and Analyzed Using RNA-Seq

Time point	Experimental group	Replicates, n
Day 0	Colonoids	3
Day 5	-endothelium/-stretch	4
	-endothelium/+stretch	4
	+endothelium/-stretch	4
	+endothelium/+stretch	6
Day 8	-endothelium/-stretch	4
	-endothelium/+stretch	4
	+endothelium/-stretch	4
	+endothelium/+stretch	3

Scanning Electron Microscopy

At the indicated time points, the Colon Intestine-Chips were fixed at room temperature for 2 hours in 2.5% glutaraldehyde solution and washed 3 times with 0.1 mol/L sodium cacodylate buffer. Concomitantly, the Chip was trimmed using a razor so that the lateral and top portions of PDMS were removed and the top channel was shown. Afterward, the samples were fixed with 1% osmium tetroxide in 0.1 mol/L sodium cacodylate buffer for 1 hour at room temperature and dehydrated in graded ethanol. The Chip samples were dried using the chemical drying agent hexamethyldisilazane, sputter-coated with platinum, and images were acquired using the Hitachi (Westford, MA) S-4700 Field Emission Scanning Electron Microscope. The morphologic analysis of the microvilli was performed according to a previously described method.⁶¹

Assessment of STAT3 Phosphorylation, Caspase 3 Cleavage, and Cytokine Secretion

At the indicated time points after stimulation with IL22 or IFN γ , the Colon Intestine-Chip was disconnected from pods, endothelial cells were removed enzymatically, and, subsequently, epithelial cells were lysed with a protein lysis buffer (R60TX-3; Meso Scale Discovery, Rockville, MD) containing protease (78425; Thermo Fisher) and phosphatase inhibitors (P0044 and P5726; Sigma-Aldrich). Protein extraction was performed according to standard protocols and the quantification of the total amount of protein/sample was performed by Bradford assay (1856210; Thermo Fisher). Total and phosphorylated STAT3 and total and cleaved caspase 3 were detected using Meso Scale Discovery

Table 4. List of Epithelial Cell Samples Treated With Various Concentrations of IL22, and Analyzed Using RNA-Seq

Time point	Experimental group	Replicates, n
Day 5	Vehicle	3
	0.01 nmol/L IL22	3
	0.1 nmol/L IL22	3
	1 nmol/L IL22	3

technology (totalSTAT3-K150SND, phosphorylatedSTAT3-K150DIA, cleaved/total-caspase 3-K15140D).

To assess the secretion of proinflammatory cytokines and acute inflammatory response proteins, effluents were collected from both channels of the Colon Intestine-Chip at the indicated time points after stimulation with IFN γ . IL6, intercellular cell adhesion molecule-1, vascular cell adhesion molecule-1, and serum amyloid A were detected using the Meso Scale Discovery technology (K15198D and K15049G; Meso Scale Discovery).

RNA Isolation, Reverse Transcription, and qPCR

Each channel of the Colon Intestine-Chip was lysed using TRI Reagent (T9424; Sigma-Aldrich) and RNA was isolated using the Direct-zol RNA Purification Kit (R2060; Zymo Research, Irvine, CA). Genomic DNA was removed using the TURBO DNA-free Kit (AM1907; Thermo Fisher), and reverse transcription to complementary DNA was performed with the SuperScript IV Synthesis System (18091050; Thermo Fischer). TaqMan Fast Advanced Master Mix (4444963; Applied Biosystems, Foster City, CA) and TaqMan Gene Expression Assays (Table 2) were used for qPCR. The qPCR was detected on a QuantStudio 3 PCR System (Thermo Fisher Scientific, Waltham, MA). The raw data were transformed to linear data by calculating the $2^{-\Delta\Delta Ct}$ values.

RNA-seq Analysis

Total RNA was extracted using TRI Reagent (T9424; Sigma-Aldrich). Bulk RNA sequencing was performed in colonoids, in suspension culture, and colonoid-derived epithelial cells cultured in the presence and absence of endothelium and/or stretch on days 5 and 8 of culture, using a minimum of 3 technical replicates per experimental group (Tables 3 and 4).

The bulk RNA sequencing platform used was the Illumina (San Diego, CA) TruSeq paired-end sequencing with a maximum read length of 2×100 bp. The sequencing depth was at approximately 48 million paired-end reads/sample. The sequence reads were trimmed using Trimmomatic v.0.36 to remove poor-quality adapter sequences and nucleotides. Using the Spliced Transcripts Alignment to a Reference aligner v.2.5.2b, we mapped the trimmed reads to the Homo sapiens reference genome GRCh38 (available on ENSEMBL) and generated the corresponding BAM and feature count files. Next, using the v.1.5.2 subread package, we calculated the gene hit counts. It is worth mentioning that only unique reads that fell within exon regions were counted. Genes with very low expressions across samples were filtered out and the remainder was used to form our data set, which was used for the differential gene expression (DGE) analysis. We performed DGE analysis using the DESeq2 R package by Bioconductor. For all but 2 DGE analyses, we applied the following widely accepted strict thresholds: $P < .01$ and $|\log_2\text{foldchange}| > 2$. A more relaxed version of these thresholds (ie, $P < .05$ and $|\log_2\text{foldchange}| > 1$) was used to identify the differentially

expressed genes in the presence and absence of stretch (Figure 5J and K).

All RNA-seq data described in this article are accessible through the Gene Expression Omnibus database (accession number: GSE179130).

Functional Enrichment Analysis

The genes identified from the DGE analysis were used to perform GO enrichment analysis with the GO biological processes. The GO term enrichment analysis was performed using the GO knowledgebase (Gene Ontology Resource available at: <http://geneontology.org>).

Statistical Analysis

Results are expressed as boxplots, depicting the minimum, first quartile, median, third quartile, and maximum values, or means \pm 95% CI and means \pm SD, as appropriate. The statistical analysis was performed using GraphPad Prism, version 8.3.0 (GraphPad Software, Inc), by applying a 2-tailed, unpaired *t* test, 1-way or 2-way analysis of variance followed by the Tukey post hoc multiple comparison tests, according to the experimental design. Any *P* value less than .05 was considered statically significant.

References

- Peterson LW, Artis D. Intestinal epithelial cells: regulators of barrier function and immune homeostasis. *Nat Rev Immunol* 2014;14:141–153.
- Sartor RB. Mechanisms of disease: pathogenesis of Crohn's disease and ulcerative colitis. *Nat Clin Pract Gastroenterol Hepatol* 2006;3:390–407.
- Camilleri M. Leaky gut: mechanisms, measurement and clinical implications in humans. *Gut* 2019;68:1516–1526.
- Bhatt AP, Gunasekara DB, Speer J, Reed MI, Peña AN, Midkiff BR, Magness ST, Bultman SJ, Allbritton NL, Redinbo MR. Nonsteroidal anti-inflammatory drug-induced leaky gut modeled using polarized monolayers of primary human intestinal epithelial cells. *ACS Infect Dis* 2018;4:46–52.
- Wang F, Graham WV, Wang Y, Witkowski ED, Schwarz BT, Turner JR. Interferon- γ and tumor necrosis factor- α synergize to induce intestinal epithelial barrier dysfunction by up-regulating myosin light chain kinase expression. *Am J Pathol* 2005;166:409–419.
- Nava P, Koch S, Laukoetter MG, Lee WY, Kolegraff K, Capaldo CT, Beeman N, Addis C, Gerner-Smidt K, Neumaier I, Skerra A, Li L, Parkos CA, Nusrat A. Interferon- γ regulates intestinal epithelial homeostasis through converging β -catenin signaling pathways. *Immunity* 2010;32:392–402.
- Madara JL, Stafford J. Interferon- γ directly affects barrier function of cultured intestinal epithelial monolayers. *J Clin Invest* 1989;83:724–727.
- Sato T, Vries RG, Snippert HJ, Van De Wetering M, Barker N, Stange DE, Van Es JH, Abo A, Kujala P, Peters PJ, Clevers H. Single Lgr5 stem cells build crypt-villus structures in vitro without a mesenchymal niche. *Nature* 2009;459:262–265.
- Sinagoga KL, Wells JM. Generating human intestinal tissues from pluripotent stem cells to study development and disease. *EMBO J* 2015;34:1149–1163.
- Cristobal A, van den Toorn HWP, van de Wetering M, Clevers H, Heck AJR, Mohammed S. Personalized proteome profiles of healthy and tumor human colon organoids reveal both individual diversity and basic features of colorectal cancer. *Cell Rep* 2017;18:263–274.
- Yu H, Hasan NM, In JG, Estes MK, Kovbasnjuk O, Zachos NC, Donowitz M. The contributions of human mini-intestines to the study of intestinal physiology and pathophysiology. *Annu Rev Physiol* 2017;79:291–312.
- Bhatia SN, Ingber DE. Microfluidic organs-on-chips. *Nat Biotechnol* 2014;32:760–772.
- Kasendra M, Tovaglieri A, Sontheimer-Phelps A, Jalili-Firoozinezhad S, Bein A, Chalkiadaki A, Scholl W, Zhang C, Rickner H, Richmond CA, Li H, Breault DT, Ingber DE. Development of a primary human Small Intestine-on-a-Chip using biopsy-derived organoids. *Sci Rep* 2018, Epub ahead of print.
- Kasendra M, Luc R, Yin J, Manatakis DV, Kulkarni G, Lucchesi C, Sliz J, Apostolou A, Sunuwar L, Obrigewitch J, Jang KJ, Hamilton GA, Donowitz M, Karalis K. Duodenum intestine-chip for preclinical drug assessment in a human relevant model. *Elife* 2020, Epub ahead of print.
- Sontheimer-Phelps A, Chou DB, Tovaglieri A, Ferrante TC, Duckworth T, Fadel C, Frisimantas V, Sutherland AD, Jalili-Firoozinezhad S, Kasendra M, Stas E, Weaver JC, Richmond CA, Levy O, Prantil-Baun R, Breault DT, Ingber DE. Human Colon-on-a-Chip enables continuous in vitro analysis of colon mucus layer accumulation and physiology. *Clin Mol Gastroenterol Hepatol* 2020, Epub ahead of print.
- Tovaglieri A, Sontheimer-Phelps A, Geirnaert A, Prantil-Baun R, Camacho DM, Chou DB, Jalili-Firoozinezhad S, De Wouters T, Kasendra M, Super M, Cartwright MJ, Richmond CA, Breault DT, Lacroix C, Ingber DE. Species-specific enhancement of enterohemorrhagic *E. coli* pathogenesis mediated by microbiome metabolites. *Microbiome* 2019, Epub ahead of print.
- Tsai PY, Zhang B, He WQ, Zha JM, Odenwald MA, Singh G, Tamura A, Shen L, Sailer A, Yeruva S, Kuo WT, Fu YX, Tsukita S, Turner JR. IL-22 upregulates epithelial claudin-2 to drive diarrhea and enteric pathogen clearance. *Cell Host Microbe* 2017, Epub ahead of print.
- Wang Y, Mumm JB, Herbst R, Kolbeck R, Wang Y. IL-22 increases permeability of intestinal epithelial tight junctions by enhancing claudin-2 expression. *J Immunol* 2017, Epub ahead of print.
- Powell N, Pantazi E, Pavlidis P, Tsakmaki A, Li K, Yang F, Parker A, Pin C, Cozzetto D, Minns D, Stolarczyk E, Saveljeva S, Mohamed R, Lavender P, Afzali B, Digby-Bell J, Tjir-Li T, Kaser A, Friedman J, MacDonald TT, Bewick GA, Lord GM. Interleukin-22 orchestrates a pathological endoplasmic reticulum stress response transcriptional programme in colonic epithelial cells. *Gut* 2019, Epub ahead of print.

20. Rothenberg ME, Wang Y, Lekkerkerker A, Danilenko DM, Maciuga R, Erickson R, Herman A, Stefanich E, Lu TT. Randomized phase I healthy volunteer study of UTTR1147A (IL-22Fc): a potential therapy for epithelial injury. *Clin Pharmacol Ther* 2019;105:177–189.
21. Brayden DJ, Maher S, Bahar B, Walsh E. Sodium caprate-induced increases in intestinal permeability and epithelial damage are prevented by misoprostol. *Eur J Pharm Biopharm* 2015, Epub ahead of print.
22. Tse CM, Yin J, Singh V, Sarker R, Lin R, Verkman AS, Turner JR, Donowitz M. cAMP stimulates SLC26A3 activity in human colon by a CFTR-dependent mechanism that does not require CFTR activity. *Clin Mol Gastroenterol Hepatol* 2019, Epub ahead of print.
23. Bechmann MB, Rotoli D, Morales M, Maeso M del C, García M del P, Ávila J, Mobasher A, Martín-Vasallo P. Na,K-ATPase isozymes in colorectal cancer and liver metastases. *Front Physiol* 2016, Epub ahead of print.
24. Watson CL, Howell JC, Schweitzer JI, Munera J, Mahe MM, Sundaram N, Vallance J, Shroyer NF, Wells JM, Helmrath MA. 925b Murine model for studying human intestine: human intestinal organoids (HIOs) engrafted in vivo develop into mature epithelial and mesenchymal intestinal tissue. *Gastroenterology* 2015, Epub ahead of print.
25. Sato T, Stange DE, Ferrante M, Vries RGJ, Van Es JH, Van Den Brink S, Van Houdt WJ, Pronk A, Van Gorp J, Siersema PD, Clevers H. Long-term expansion of epithelial organoids from human colon, adenoma, adenocarcinoma, and Barrett's epithelium. *Gastroenterology* 2011, Epub ahead of print.
26. Basak O, Beumer J, Wiebrands K, Seno H, van Oudenaarden A, Clevers H. Induced quiescence of Lgr5+ stem cells in intestinal organoids enables differentiation of hormone-producing enteroendocrine cells. *Cell Stem Cell* 2017, Epub ahead of print.
27. Neurath MF. Cytokines in inflammatory bowel disease. *Nat Rev Immunol* 2014, Epub ahead of print.
28. Bruewer M, Luegering A, Kucharzik T, Parkos CA, Madara JL, Hopkins AM, Nusrat A. Proinflammatory cytokines disrupt epithelial barrier function by apoptosis-independent mechanisms. *J Immunol* 2003, Epub ahead of print.
29. Jones S, Banks R, Haidar A, Gearing A, Hemingway I, Ibbotson S, Dixon M, Axon A. Adhesion molecules in inflammatory bowel disease. *Gut* 1995;36:724–730.
30. Uhlar CM, Whitehead AS. Serum amyloid A, the major vertebrate acute-phase reactant. *Eur J Biochem* 1999, Epub ahead of print.
31. Kamanaka M, Huber S, Zenewicz LA, Gagliani N, Rathinam C, O'Connor W, Wan YY, Nakae S, Iwakura Y, Hao L, Flavell RA. Memory/effector (CD45RBlo) CD4 T cells are controlled directly by IL-10 and cause IL-22-dependent intestinal pathology. *J Exp Med* 2011, Epub ahead of print.
32. Zenewicz LA, Yancopoulos GD, Valenzuela DM, Murphy AJ, Karow M, Flavell RA. Interleukin-22 but not interleukin-17 provides protection to hepatocytes during acute liver inflammation. *Immunity* 2007, Epub ahead of print.
33. Sabat R, Ouyang W, Wolk K. Therapeutic opportunities of the IL-22-IL-22R1 system. *Nat Rev Drug Discov* 2014, Epub ahead of print.
34. Zhang X, Liu S, Wang Y, Hu H, Li L, Wu Y, Cao D, Cai Y, Zhang J, Zhang X. Interleukin-22 regulates the homeostasis of the intestinal epithelium during inflammation. *Int J Mol Med* 2019, Epub ahead of print.
35. Zhang Xinyan, Liu Shijie, Wang Yueqian, Hu Huiqiong, Li Liang, Wu Yibin, Cao Duo, Cai Yuankun, Jiqin Zhang XZ. Interleukin-22 regulates the homeostasis of the intestinal epithelium during inflammation. *Int J Mol Med* 2019;43:1657–1668.
36. Zindl CL, Lai JF, Lee YK, Maynard CL, Harbour SN, Ouyang W, Chaplin DD, Weaver CT. IL-22-producing neutrophils contribute to antimicrobial defense and restitution of colonic epithelial integrity during colitis. *Proc Natl Acad Sci U S A* 2013, Epub ahead of print.
37. Lindemans CA, Calafiore M, Mertelsmann AM, O'Connor MH, Dudakov JA, Jenq RR, Velardi E, Young LF, Smith OM, Lawrence G, Ivanov JA, Fu YY, Takashima S, Hua G, Martin ML, O'Rourke KP, Lo YH, Mokry M, Romera-Hernandez M, Cupedo T, Dow LE, Nieuwenhuis EE, Shroyer NF, Liu C, Kolesnick R, Van Den Brink MRM, Hanash AM. Interleukin-22 promotes intestinal-stem-cell-mediated epithelial regeneration. *Nature* 2015, Epub ahead of print.
38. Peery AF, Crockett SD, Barritt AS, Dellon ES, Eluri S, Gangarosa LM, Jensen ET, Lund JL, Pasricha S, Runge T, Schmidt M, Shaheen NJ, Sandler RS. Burden of gastrointestinal, liver, and pancreatic diseases in the United States. *Gastroenterology* 2015, Epub ahead of print.
39. Sato T, Clevers H. Growing self-organizing mini-guts from a single intestinal stem cell: Mechanism and applications. *Science* 2013, Epub ahead of print.
40. Kozuka K, He Y, Koo-McCoy S, Kumaraswamy P, Nie B, Shaw K, Chan P, Leadbetter M, He L, Lewis JG, Zhong Z, Charmot D, Balaa M, King AJ, Caldwell JS, Siegel M. Development and characterization of a human and mouse intestinal epithelial cell monolayer platform. *Stem Cell Rep* 2017, Epub ahead of print.
41. In J, Foulke-Abel J, Zachos NC, Hansen AM, Kaper JB, Bernstein HD, Halushka M, Blutt S, Estes MK, Donowitz M, Kovbasnjuk O. Enterohemorrhagic *Escherichia coli* reduces mucus and intermicrovillar bridges in human stem cell-derived colonoids. *Clin Mol Gastroenterol Hepatol* 2016, Epub ahead of print.
42. Bonnans C, Chou J, Werb Z. Remodelling the extracellular matrix in development and disease. *Nat Rev Mol Cell Biol* 2014, Epub ahead of print.
43. Wang Y, Kim R, Gunasekara DB, Reed MI, DiSalvo M, Nguyen DL, Bultman SJ, Sims CE, Magness ST, Allbritton NL. Formation of human colonic crypt array by application of chemical gradients across a shaped epithelial monolayer. *Clin Mol Gastroenterol Hepatol* 2018, Epub ahead of print.

44. Langer V, Vivi E, Regensburger D, Winkler TH, Waldner MJ, Rath T, Schmid B, Skottke L, Lee S, Jeon NL, Wohlfahrt T, Kramer V, Tripal P, Schumann M, Kersting S, Handtrack C, Geppert CI, Suchowski K, Adams RH, Becker C, Ramming A, Naschberger E, Britzen-Laurent N, Stürzl M. IFN- γ drives inflammatory bowel disease pathogenesis through VE-cadherin-directed vascular barrier disruption. *J Clin Invest* 2019, Epub ahead of print.
45. Wang F, Schwarz BT, Graham WV, Wang Y, Su L, Clayburgh DR, Abraham C, Turner JR. IFN- γ -induced TNFR2 upregulation is required for TNF-dependent intestinal epithelial barrier dysfunction. *Gastroenterology* 2006;131:1153–1163.
46. Mizuno S, Mikami Y, Kamada N, Handa T, Hayashi A, Sato T, Matsuoka K, Matano M, Ohta Y, Sugita A, Koganei K, Sahara R, Takazoe M, Hisamatsu T, Kanai T. Cross-talk between ROR γ t⁺ innate lymphoid cells and intestinal macrophages induces mucosal IL-22 production. In *Crohn's disease. Inflamm Bowel Dis* 2014, Epub ahead of print.
47. Victor AR, Nalin AP, Dong W, McClory S, Wei M, Mao C, Kladney RD, Youssef Y, Chan WK, Brierecheck EL, Hughes T, Scoville SD, Pitarresi JR, Chen C, Manz S, Wu L-C, Zhang J, Ostrowski MC, Freud AG, Leone GW, Caligiuri MA, Yu J. IL-18 drives ILC3 proliferation and promotes IL-22 production via NF- κ B. *J Immunol* 2017, Epub ahead of print.
48. Backert I, Korolov SB, Wirtz S, Kitowski V, Billmeier U, Martini E, Hofmann K, Hildner K, Wittkopf N, Brecht K, Waldner M, Rajewsky K, Neurath MF, Becker C, Neufert C. STAT3 activation in Th17 and Th22 cells controls IL-22-mediated epithelial host defense during infectious colitis. *J Immunol* 2014, Epub ahead of print.
49. Dige A, Støy S, Rasmussen TK, Kelsen J, Hvas CL, Sandahl TD, Dahlerup JF, Deleuran B, Agnholt J. Increased levels of circulating Th17 cells in quiescent versus active Crohn's disease. *J Crohn's Colitis* 2013, Epub ahead of print.
50. Sipponen P, Hyvärinen H. Role of helicobacter pylori in the pathogenesis of gastritis, peptic ulcer and gastric cancer. *Scand J Gastroenterol* 1993, Epub ahead of print.
51. Wolk K, Witte E, Wallace E, Döcke WD, Kunz S, Asadullah K, Volk HD, Sterry W, Sabat R. IL-22 regulates the expression of genes responsible for antimicrobial defense, cellular differentiation, and mobility in keratinocytes: a potential role in psoriasis. *Eur J Immunol* 2006, Epub ahead of print.
52. Zheng Y, Valdez PA, Danilenko DM, Hu Y, Sa SM, Gong Q, Abbas AR, Modrusan Z, Ghilardi N, De Sauvage FJ, Ouyang W. Interleukin-22 mediates early host defense against attaching and effacing bacterial pathogens. *Nat Med* 2008, Epub ahead of print.
53. Hoegl S, Bachmann M, Scheiermann P, Goren I, Hofstetter C, Pfeilschifter J, Zwissler B, Muhl H. Protective properties of inhaled IL-22 in a model of ventilator-induced lung injury. *Am J Respir Cell Mol Biol* 2011, Epub ahead of print.
54. Sugimoto K, Ogawa A, Mizoguchi E, Shimomura Y, Andoh A, Bhan AK, Blumberg RS, Xavier RJ, Mizoguchi A. IL-22 ameliorates intestinal inflammation in a mouse model of ulcerative colitis. *J Clin Invest* 2008, Epub ahead of print.
55. Bachmann M, Ulziibat S, Härdle L, Pfeilschifter J, Muhl H. IFN α converts IL-22 into a cytokine efficiently activating STAT1 and its downstream targets. *Biochem Pharmacol* 2013, Epub ahead of print.
56. Herrero C, Hu X, Li WP, Samuels S, Sharif MN, Kotenko S, Ivashkiv LB. Reprogramming of IL-10 activity and signaling by IFN- γ . *J Immunol* 2003, Epub ahead of print.
57. Khare V, Paul G, Movadat O, Frick A, Jambrich M, Krnjic A, Marian B, Wrba F, Gasche C. IL10R2 over-expression promotes IL22/STAT3 signaling in colorectal carcinogenesis. *Cancer Immunol Res* 2015, Epub ahead of print.
58. Brand S, Beigel F, Olszak T, Zitzmann K, Eichhorst ST, Otte JM, Diepolder H, Marquardt A, Jagla W, Popp A, Leclair S, Herrmann K, Seiderer J, Ochsenkühn T, Göke B, Auernhammer CJ, Dambacher J. IL-22 is increased in active Crohn's disease and promotes proinflammatory gene expression and intestinal epithelial cell migration. *Am J Physiol Gastrointest Liver Physiol* 2006, Epub ahead of print.
59. Martin JC, Bériou G, Heslan M, Chauvin C, Utraiainen L, Aumeunier A, Scott CL, Mowat A, Cerovic V, Houston SA, Leboeuf M, Hubert FX, Hémond C, Merad M, Milling S, Josien R. Interleukin-22 binding protein (IL-22BP) is constitutively expressed by a subset of conventional dendritic cells and is strongly induced by retinoic acid. *Mucosal Immunol* 2014, Epub ahead of print.
60. Martin JC, Bériou G, Heslan M, Bossard C, Jarry A, Abidi A, Hulin P, Ménoret S, Thinard R, Anegon I, Jacqueline C, Lardeux B, Halary F, Renauld J-C, Bourreille A, Josien R. IL-22BP is produced by eosinophils in human gut and blocks IL-22 protective actions during colitis. *Mucosal Immunol* 2016;9:539–549.
61. Gemma J, Ma Dolores M, Marc C, Miquel R. Image processing techniques to quantify microprojections on outer corneal epithelial cells. *J Anat* 2008;212:879–886.

Received October 21, 2020. Accepted July 6, 2021.

Correspondence

Address correspondence to: Katia Karalis, MD, PhD, Regeneron Pharmaceuticals, RGC, 87 Coolidge Street, Brookline, Massachusetts 02446. e-mail: katia.karalis@regeneron.com.

Acknowledgments

The authors would like to thank Professor Mark Donowitz for providing the colonic organoid samples. The authors also thank Brett Clair for scientific illustrations.

Human tissue samples were obtained from John Hopkins University, Professor Mark Donowitz's laboratory, under the enclosed Material Transfer Agreement.

The graphical abstracts were created using Adobe Illustrator CC 2021 (25.2.3) and CINEMA 4D (MAXON computer).

CRedit Authorship Contributions

Athanasia Apostolou, PhD (Data curation: Lead; Formal analysis: Lead; Investigation: Lead; Methodology: Equal; Visualization: Lead; Writing – original draft: Supporting; Experimental Planning: Lead)

Rohit A. Panchakshari, PhD (Data curation: Equal; Formal analysis: Equal; Methodology: Equal; Writing – review & editing: Equal; Experimental Planning: Equal)

Antara Banerjee, PhD (Methodology: Equal; Writing – review & editing: Supporting; Experimental Planning: Equal)

Dimitris V. Manatakis, PhD (Data curation: Equal; Formal analysis: Equal; Methodology: Equal; Visualization: Equal; Writing – review & editing: Supporting)

Maria D. Paraskevopoulou, PhD (Data curation: Lead; Formal analysis: Equal; Methodology: Equal; Visualization: Equal; Writing – review & editing: Equal)

Raymond Luc, MSc (Data curation: Equal; Investigation: Equal; Methodology: Equal; Writing – review & editing: Supporting)

Galeb Abu-Ali, PhD (Formal analysis: Supporting)

Alexandra Dimitriou, MSc (Investigation: Supporting)

Carolina Lucchesi, PhD (Investigation: Supporting)

Gauri Kulkarni, MSc (Investigation: Supporting)

Tengku Ibrahim Maulana, MSc (Investigation: Supporting)

Magdalena Kasendra, PhD (Data discussion: Supporting)

Jordan S. Kerns, PhD (Data discussion: Supporting)

Bertram Bleck, PhD (Writing – review & editing: Equal)

Lorna Ewart, PhD (Writing – review & editing: Equal)

Elias S. Manolagos, PhD (Formal analysis: Lead; Methodology: Equal; Writing – review & editing: Equal)

Geraldine A. Hamilton, PhD (Writing – review & editing: Supporting)

Cosmas Giallourakis, MD (Conceptualization: Equal; Supervision: Equal; Writing – review & editing: Equal)

Katia Karalis, MD, PhD (Conceptualization: Equal; Supervision: Lead; Writing – review & editing: Lead)

Conflicts of interest

These authors disclose the following: Athanasia Apostolou, Dimitris V. Manatakis, Raymond Luc, Alexandra Dimitriou, Carolina Lucchesi, Gauri Kulkarni, Lorna Ewart, Magdalena Kasendra, Jordan S. Kerns, Geraldine A. Hamilton, and Katia Karalis are current or former employees of Emulate, Inc, and may hold equity interest in Emulate, Inc; and Rohit A. Panchakshari, Antara Banerjee, Maria D. Paraskevopoulou, Galeb Abu-Ali, Bertram Bleck, and Cosmas Giallourakis are current or former employees of Takeda Pharmaceutical Company, Ltd, and may hold equity interest in Takeda Pharmaceutical Company, Ltd. The remaining authors disclose no conflicts.

Funding

This project was co-funded by Emulate, Inc, and Takeda Pharmaceutical Company, Ltd.